NASA TECHNICAL NOTE

NASA TN D-8107 c.1

NASA TN D-8107

NUCLEON AND HEAVY-ION TOTAL AND ABSORPTION CROSS SECTION FOR SELECTED NUCLEI

John W. Wilson and Christopher M. Costner

Langley Research Center
Hampton, Va. 23665

NATIONAL AERONAUTICS AND SPACE ADMINISTRATION • WASHINGTON, D. C. • DECEMBER 1975

1. Report No. NASA TN D-8107	2. Government Accession No.	3. Recipient's Catalog No.
4. Title and Subtitle NUCLEON AND HEAVY-ION TOTAL AND ABSORPTION CROSS SECTION FOR SELECTED NUCLEI		5. Report Date December 1975
		6. Performing Organization Code
7. Author(s) John W. Wilson and Christopher M. Costner		8. Performing Organization Report No. L-10547
		10. Work Unit No. 505-08-10-01
9. Performing Organization Name and Address NASA Langley Research Center Hampton, Va. 23665		11. Contract or Grant No.
		13. Type of Report and Period Covered Technical Note
12. Sponsoring Agency Name and Address National Aeronautics and Space Administration Washington, D.C. 20546		14. Sponsoring Agency Code
15. Supplementary Notes John W. Wilson: Langley Research Center. Christopher M. Costner: Old Dominion University, Norfolk, Virginia.		

16. Abstract

Approximate solutions of the coupled-channel equations for high-energy composite particle scattering are obtained and are applied to the nuclear scattering problem. Relationships between several approximation procedures are established and discussed. The eikonal formalism is used with a small-angle approximation to calculate the coherent elastic scattered amplitude from which total and absorption cross sections are derived. Detailed comparisons with nucleon-nucleus experiments show agreement within 5 percent except at lower energies where the eikonal approximation is of questionable accuracy. Even at these lower energies, agreement is within 15 percent. Tables of cross sections required for cosmic heavy-ion transport and shielding studies are presented.

17. Key Words (Suggested by Author(s)) Heavy ion Nuclear reactions Cosmic rays Scattering theory		18. Distribution Statement Unclassified – Unlimited Subject Category 73	
19. Security Classif. (of this report) Unclassified	20. Security Classif. (of this page) Unclassified	21. No. of Pages 77	22. Price* $4.75

*For sale by the National Technical Information Service, Springfield, Virginia 22161

NUCLEON AND HEAVY-ION TOTAL AND ABSORPTION CROSS SECTION FOR SELECTED NUCLEI

John W. Wilson and Christopher M. Costner*
Langley Research Center

SUMMARY

Approximate solutions of the coupled-channel equations for high-energy composite particle scattering are obtained and are applied to the nuclear scattering problem. Relationships between several approximation procedures are established and discussed. The eikonal formalism is used with a small-angle approximation to calculate the coherent elastic scattered amplitude from which total and absorption cross sections are derived. Detailed comparisons with nucleon-nucleus experiments show agreement within 5 percent except at lower energies where the eikonal approximation is of questionable accuracy. Even at these lower energies, agreement is within 15 percent. Tables of cross sections required for cosmic heavy-ion transport and shielding studies are presented.

INTRODUCTION

The high-energy heavy ions of the cosmic radiation pose an ever-present hazard to spacecraft and high-altitude aircraft. In particular, for manned space missions of long duration or for crew members of high-altitude aircraft flight in which career lifetimes may approach 25 years, the potential adverse effects on nonregenerative tissues are of extreme importance. (See refs. 1 and 2.) Because the range of such energetic particles is large compared with spacecraft walls and with the overhead air mass at very high altitudes, an attractive means of radiation protection appears to be through attenuation and breakup in nuclear reaction. To make effective use of nuclear attenuation, the corresponding cross sections must be accurately known since even modest cross-section uncertainty can, because of the exponential relation of cross section to transmitted primary flux, produce large errors in such calculations. For example, a 25-percent uncertainty in absorption cross section produces an order of magnitude uncertainty in flux after only three mean free paths. In addition, the uncertainty in production cross sections for the reaction products produces further uncertainty in the transmitted flux. This resultant flux uncertainty may also be large as demonstrated by Curtis and Wilkinson. (See ref. 3.)

*Old Dominion University, Norfolk, Virginia.

In the present report, a recent high-energy heavy-ion reaction model for potential use in estimating the required nuclear parameters is discussed. (See refs. 4 and 5.) The model consists of a coupled-channel Schroedinger equation derived under the assumption of high-energy and closure of the internal nuclear states. Approximation procedures for solution of the coupled equations and examination of the lowest order approximation are contained. Comparisons with available nuclear cross-sectional measurements are made. Extensive tables of heavy-ion cross sections required for cosmic-ray shielding studies are presented.

SYMBOLS

A	nuclear mass number, dimensionless
a	parameter in Woods-Saxon function, fm
a_C,R	parameters for Woods-Saxon charge density, fm
$a_{P,\ell}$	ℓth transition moment of projectile, $(\mathrm{fm})^{\ell}$
$a_{T,\ell}$	ℓth transition moment of target, $(\mathrm{fm})^{\ell}$
a_p	proton root-mean-square charge radius, fm
$B(e)$	average of slope parameters of nucleon-nucleon scattering amplitude, $(\mathrm{fm})^2$
B_{pp},B_{np}	slope parameter for proton-proton and neutron-proton scattering, $(\mathrm{fm})^2$
$\vec{b}$	projectile impact parameter vector, fm
E	projectile laboratory energy per unit mass, GeV/amu
e	two-nucleon kinetic energy in their center-of-mass frame, MeV
$F(\vec{q})$	nuclear form factor, dimensionless
$\bar{f}(\vec{q})$	heavy-ion scattering amplitude, fm
$\bar{f}^B(\vec{q})$	Born approximation to $\bar{f}(\vec{q})$, fm

$f(e,\vec{q})$	average two-nucleon scattering amplitude, fm
$f_c(\vec{q})$	heavy-ion coherent scattering amplitude, fm
$f_i(e,\vec{q})$	for $i = pp,np$ two-nucleon scattering amplitude, fm
G_c	coherent propagator or coherent Green's function, dimensionless
$g_{P,m}\left(\vec{\xi}_P\right)$	projectile internal wave function for state m, $(fm)^{-3/2}$
$g_{T,\mu}\left(\vec{\xi}_T\right)$	target internal wave function for state μ, $(fm)^{-3/2}$
J_m, J_μ	total internal angular momentum quantum numbers for projectile in state m and target in state μ, dimensionless
$\vec{k}$	projectile momentum vector relative to target in initial state, $(fm)^{-1}$
$\vec{k}_f$	projectile momentum vector relative to target in final state, $(fm)^{-1}$
ℓ	orbital angular momentum quantum number, dimensionless
m	nucleon mass, 938 MeV/c^2
N	total number of nuclear constituents, dimensionless
N_P, N_T	neutron numbers of projectile and target, dimensionless
$\vec{q}$	momentum transfer vector ($\vec{q} = \vec{k}_f - \vec{k}$), $(fm)^{-1}$
$\vec{r}$	position vector relative to nuclear center of mass, fm
r_u	nuclear equivalent uniform radius, fm
$r_{0.5}$	nuclear half-density radius and equal to R, fm
t	nuclear skin thickness, fm
$\tilde{t}$	average two-nucleon transition amplitudes, MeV

t_C nuclear charge skin thickness, fm

t_{nn}, t_{pp}, t_{np} two-nucleon transition amplitudes for neutron-neutron, proton-proton, and neutron-proton scattering, MeV

$t_{\alpha j}\left(\vec{x}_\alpha, \vec{x}_j\right)$ two-nucleon transition operator for nucleons α and j at positions $\vec{x}_\alpha$ and $\vec{x}_j$, MeV

$\overline{U}(\vec{x})$ optical potential matrix, $(MeV)^2$

$U_c(\vec{x})$ coeherent optical potential, $(MeV)^2$

$V_{m\mu, m'\mu'}(\vec{x})$ matrix elements of optical potential operator, MeV

$V_{opt}\left(\vec{\xi}_P, \vec{\xi}_T, \vec{x}\right)$ optical potential operator, MeV

$\vec{x}$ relative position vector of projectile ($\vec{x} = \vec{b} + \vec{z}$), fm

$\vec{y}$ two-nucleon relative position vector, fm

z projection of $\vec{x}$ along beam, fm

$\hat{z}$ unit vector along beam, dimensionless

α_{pp}, α_{np} ratio of real to imaginary parts of proton-proton and neutron-proton scattering amplitudes, dimensionless

$\bar{\delta}$ entrance channel unit vector, dimensionless

θ scattering angle, radians

$\vec{\xi}_P, \vec{\xi}_T$ collections of constituent relative coordinates for projectile and target, fm

$\rho_A(\vec{r})$ nuclear single-particle density, $(fm)^{-3}$

$\rho_{C,A}(\vec{r})$ nuclear charge density, $(fm)^{-3}$

$\rho_{C,p}(\vec{r})$ proton charge density, $(fm)^{-3}$

$\rho_n(\vec{r}), \rho_p(\vec{r})$	neutron and proton densities in nucleus, $(fm)^{-3}$
σ_{pp}, σ_{np}	proton-proton and neutron-proton total cross sections, $(fm)^2$ or (mb)
$\sigma_{tot}, \sigma_s, \sigma_{abs}$	heavy-ion total, scattering, and absorption cross sections, $(fm)^2$ or (mb)
$\overline{\phi}(\vec{x})$	coupled-channel phase operator, dimensionless
$\bar{\chi}(\vec{b})$	eikonal phase shift, dimensionless
$\overline{\psi}(\vec{x})$	coupled-channel scattered wave, $(fm)^{-3/2}$
$\overline{\psi}_i(\vec{x})$	ith term of multiple-excitation series for $\overline{\psi}(\vec{x})$
$\overline{\psi}^{(i)}(\vec{x})$	ith iterate of perturbation approximation to $\overline{\psi}(\vec{x})$
$\psi_{m\mu}(\vec{x})$	components of $\overline{\psi}(\vec{x})$
$\overline{\psi}_p(\vec{x})$	entering plane wave state, $(fm)^{-3/2}$
Ω	coupled-channel wave operator, dimensionless
Ω_c	coherent wave operator, dimensionless

Subscripts:

m	internal quantum numbers of projectile
P	projectile
T	target
μ	internal quantum numbers of target

Superscript:

*	complex conjugate

Arrows indicate vectors.

HEAVY-ION DYNAMICAL EQUATIONS

In this section, the coupled-channel equations for composite particle scattering are examined. Particular attention is given to the relation between the coherent elastic scattered wave, the Born approximation, Chew's form of the impulse approximation (ref. 6), the distorted-wave Born approximation (DWBA) (ref. 7), and various approximation procedures to the coupled equations. Finally, it will be shown how the coupled equations can be solved by using the eikonal approximation, and a simplified expression for the scattering amplitude is derived that includes the elastic and all the inelastic scattering amplitudes for small scattering angles. Discussion of the usual use of the optical theorem to estimate total cross sections from the coherent elastic scattered wave will shed some light on the reasons that this estimate of total cross section is successful.

Coupled-Channel Equations

The starting point for the present discussion is the coupled-channel (Schroedinger) equation relating the entrance channel to all excited states of the target and projectile. This equation was derived by assuming the kinetic energy to be large compared with the excitation energy of the target and projectile and closure for the accessible internal eigenstates. (See refs. 4 and 5.) These coupled equations are given as

$$\left(\nabla_x^2 + \vec{k}^2\right)\psi_{m\mu}(\vec{x}) = \left(\frac{2mA_PA_T}{N}\right)\sum_{m'\mu'} V_{m\mu,m'\mu'}(\vec{x})\ \psi_{m'\mu'}(\vec{x}) \tag{1}$$

where subscripts m and μ label the eigenstates of the projectile and target, A_P and A_T are projectile and target mass number, m is constituent mass, $\vec{k}$ is projectile momentum relative to the center of mass, $\vec{x}$ is the projectile position vector relative to the target, with

$$V_{m\mu,m'\mu'}(\vec{x}) = \left\langle g_{P,m}\left(\vec{\xi}_P\right)\ g_{T,\mu}\left(\vec{\xi}_T\right)\middle| V_{opt}\left(\vec{\xi}_P,\vec{\xi}_T,\vec{x}\right)\middle| g_{P,m'}\left(\vec{\xi}_P\right)\ g_{T,\mu'}\left(\vec{\xi}_T\right)\right\rangle \tag{2}$$

The quantities $g_{P,m}\left(\vec{\xi}_P\right)$ and $g_{T,\mu}\left(\vec{\xi}_T\right)$ are the projectile and target internal wave functions, $\vec{\xi}_P$ and $\vec{\xi}_T$ are collections of internal coordinates of the projectile and target constituents, $V_{opt}\left(\vec{\xi}_P,\vec{\xi}_T,\vec{x}\right)$ is the effective potential operator derived in reference 4 and given by

$$V_{opt}\left(\vec{\xi}_P,\vec{\xi}_T,\vec{x}\right) = \sum_{\alpha j} t_{\alpha j}\left(\vec{x}_\alpha,\vec{x}_j\right) \tag{3}$$

Here, $t_{\alpha j}\left(\vec{x}_\alpha,\vec{x}_j\right)$ is the two-body transition operator for the j-constituent of the projectile at position $\vec{x}_j$ and the α-constituent of the target at $\vec{x}_\alpha$. The N is the total constituent number defined as

$$N = A_P + A_T \tag{4}$$

The notation is simplified by introducing the wave vector

$$\bar{\psi}(\vec{x}) = \begin{bmatrix} \psi_{00}(\vec{x}) \\ \psi_{01}(\vec{x}) \\ \psi_{10}(\vec{x}) \\ \psi_{11}(\vec{x}) \\ \cdot \\ \cdot \\ \cdot \end{bmatrix} \tag{5}$$

and the potential matrix

$$\bar{U}(\vec{x}) = \left(\frac{2mA_TA_P}{N}\right) \begin{bmatrix} V_{00,00}(\vec{x}) & V_{00,01}(\vec{x}) & V_{00,10}(\vec{x}) & \cdots \\ V_{01,00}(\vec{x}) & V_{01,01}(\vec{x}) & V_{01,10}(\vec{x}) & \cdots \\ V_{10,00}(\vec{x}) & V_{10,01}(\vec{x}) & V_{10,10}(\vec{x}) & \cdots \\ V_{11,00}(\vec{x}) & V_{11,01}(\vec{x}) & V_{11,10}(\vec{x}) & \cdots \\ \cdot & \cdot & \cdot & \cdot \\ \cdot & \cdot & \cdot & \cdot \\ \cdot & \cdot & \cdot & \cdot \end{bmatrix} \tag{6}$$

The coupled equations are then written in matrix form as

$$\left(\nabla_x^{\,2} + \vec{k}^{\,2}\right)\bar{\psi}(\vec{x}) = \bar{U}(\vec{x})\ \bar{\psi}(\vec{x}) \tag{7}$$

for which the approximate solution is considered.

The object of the solution of equation (7) is the calculation of the scattering amplitude given by

$$\bar{f}(\vec{q}) = -\sqrt{\frac{\pi}{2}} \int \exp\left(-i\vec{k}_f \cdot \vec{x}\right) \bar{U}(\vec{x})\ \bar{\psi}(\vec{x})\ d^3\vec{x} \tag{8}$$

where $\vec{k}_f$ is the final projectile momentum and $\vec{q}$ is the momentum transfer vector

$$\vec{q} = \vec{k}_f - \vec{k} \tag{9}$$

Since equation (7) cannot be solved in general, the remainder of this section is devoted to the study of approximation procedures for evaluation of equation (8). To gain insight, the simplest approximations are examined first and provide a basis for more accurate and complex procedures.

Born Approximation

The Born approximation is obtained by approximating $\bar{\psi}(\vec{x})$ by the incident plane wave. The coupled amplitude is then written as

$$\bar{f}^{B}(\vec{q}) = -\frac{1}{4\pi} \int \exp\left(-i\vec{q} \cdot \vec{x}\right) \bar{U}(\vec{x})\ d^3\vec{x} \tag{10}$$

which is a matrix of approximate scattering amplitudes relating all possible entrance channels to all possible final channels. For example, diagonal elements relate to all possible elastic scatterings of the system where the elastic channel is defined by the entrance channel. Using the definition of the potential given in equations (2) and (3) results in

$$V_{m\mu,m'\mu'}(\vec{x}) = \sum_{\alpha j} \left\langle g_{P,m}\left(\vec{\xi}_P\right) g_{T,\mu}\left(\vec{\xi}_T\right) \middle| t_{\alpha j}\left(\vec{x}_\alpha, \vec{x}_j\right) \middle| g_{P,m'}\left(\vec{\xi}_P\right) g_{T,\mu'}\left(\vec{\xi}_T\right) \right\rangle$$

$$= \sum_{\alpha j} \int \rho_{T,\mu\mu'}\left(\vec{r}_\alpha\right) t_{\alpha j}\left(\vec{x}_\alpha, \vec{x}_j\right) \rho_{P,mm'}\left(\vec{r}_j\right) d^3\vec{r}_\alpha\ d^3\vec{r}_j \tag{11}$$

where

$$\rho_{P,mm'}\left(\vec{r}_j\right) = \int g^*_{P,m}\left(\vec{\xi}_P\right) \delta^3\left(\vec{r}_j - \vec{\xi}_{P,j}\right) g_{P,m'}\left(\vec{\xi}_P\right) d^3\vec{\xi}_P \tag{12}$$

and

$$\rho_{T,\mu\mu'}\left(\vec{r}_\alpha\right) = \int g^*_{T,\mu}\left(\vec{\xi}_T\right) \delta^3\left(\vec{r}_\alpha - \vec{\xi}_{T,\alpha}\right) g_{T,\mu'}\left(\vec{\xi}_T\right) d^3\vec{\xi}_T \tag{13}$$

The Fourier transform of equation (11) yields

$$\int V_{m\mu,m'\mu'}(\vec{x}) \exp(-i\vec{q} \cdot \vec{x}) \, d^3\vec{x}$$

$$= \sum_{\alpha j} \int \exp(-i\vec{q} \cdot \vec{x}) \left[\int \rho_{T,\mu\mu'}\left(\vec{r}_\alpha\right) \rho_{P,mm'}\left(\vec{r}_j\right) t_{\alpha j}\left(\vec{x}_\alpha, \vec{x}_j\right) d^3\vec{r}_\alpha \, d^3\vec{r}_j\right] d^3\vec{x}$$

$$= \sum_{\alpha j} t_{\alpha j}(k,\vec{q}) \, F_{T,\mu\mu'}(\vec{q}) \, F_{P,mm'}(-\vec{q}) \tag{14}$$

where the fact that the transition amplitudes $t_{\alpha j}\left(\vec{x}_\alpha, \vec{x}_j\right)$ depend only on the relative position vector of the α- and j-constituents relative to one another has been used. The form factors $F_{T,\mu\mu'}(\vec{q})$ and $F_{P,mm'}(\vec{q})$ are the Fourier transforms of the corresponding single-particle transition densities given in equations (12) and (13). Using equations (6) and (14) in equation (10) results in the following form for the Born approximation:

$$\bar{f}^{B}_{m'\mu',m\mu}(\vec{q}) = -\frac{1}{4\pi}\left(\frac{2mA_P{}^2A_T{}^2}{N}\right) F_{T,\mu'\mu}(\vec{q}) \, F_{P,m'm}(-\vec{q}) \, \tilde{t}(k,\vec{q}) \tag{15}$$

where

$$\tilde{t}(k,\vec{q}) = \frac{1}{A_P A_T} \sum_{\alpha j} t_{\alpha j}(k,\vec{q}) \tag{16}$$

is the transition amplitude averaged over nuclear constituents.

Consider now the projectile form factor given by the Fourier transform of the single-particle densities as

$$F_{P,m'm}(\vec{q}) = \int \exp\left(i\vec{q} \cdot \vec{r}_\alpha\right) \rho_{P,m'm}\left(\vec{r}_\alpha\right) d^3\vec{r}_\alpha$$

$$= \int g^*_{P,m'}\left(\vec{\xi}_P\right) \exp\left(i\vec{q} \cdot \vec{\xi}_{P,\alpha}\right) g_{P,m}\left(\vec{\xi}_P\right) d^3\vec{\xi}_P \tag{17}$$

Expanding the exponential factor as a power series results in

$$F_{P,m'm}(\vec{q}) = \delta_{m'm} + i\vec{a}_{P,1} \cdot \vec{q} - \frac{1}{2}\vec{q} \cdot \overleftrightarrow{a}_{P,2} \cdot \vec{q} + \ldots \tag{18}$$

where the first term in equation (18) corresponds to the normalization condition of the eigenstates, the second term contains the dipole transition moment given by

$$\vec{a}_{P,1} = \left\langle g_{P,m'}\left(\vec{\xi}_P\right) \middle| \vec{\xi}_{P,\alpha} \middle| g_{P,m}\left(\vec{\xi}_P\right) \right\rangle \tag{19}$$

and the third term contains the dyadic quadrupole transition moment

$$\overleftrightarrow{a}_{P,2} = \left\langle g_{P,m'}\left(\vec{\xi}_P\right) \middle| \vec{\xi}_{P,\alpha}\vec{\xi}_{P,\alpha} \middle| g_{P,m}\left(\vec{\xi}_P\right) \right\rangle \tag{20}$$

The higher order multipole transitions are indicated by dots in equation (18). The lowest order nonzero term in equation (18) depends on the properties of the internal wave functions involved. In general, the ℓth transition moment with magnitude given by

$$a_{P,\ell} = \left| \left\langle g_{P,m'}\left(\vec{\xi}_P\right) \middle| \left(\vec{\xi}_{P,\alpha}\right)^\ell \middle| g_{P,m}\left(\vec{\xi}_P\right) \right\rangle \right| \tag{21}$$

is zero unless

$$\left|J_{m'} - J_m\right| \leqq \ell \leqq \left|J_{m'} + J_m\right| \tag{22}$$

as a result of the Wigner-Eckart theorem where J_m and $J_{m'}$ are the projectile internal angular momentum in the entering and final states. Because of the orthogonality, equation (21) reduces to .

$$a_{P,0} = \delta_{m'm} \tag{23}$$

for $\ell = 0$. It follows from relations (22) and (23) and for small momentum transfer that

$$F_{P,m'm}(\vec{q}) \approx \delta_{m'm} + \frac{a_{P,\ell_P}\left|\vec{q}\right|^{\ell_P} i^{\ell_P}}{\ell_P!} \tag{24}$$

where

$$\ell_P = \mathrm{Max}\left\{\left|J_{m'} - J_m\right|, 1\right\} \tag{25}$$

is the angular momentum associated with the lowest order transition moment. Similarly, for the target, one obtains

$$F_{T,\mu'\mu}(\vec{q}) \approx \delta_{\mu'\mu} + \frac{a_{T,\ell_T}\left|\vec{q}\right|^{\ell_T} i^{\ell_T}}{\ell_T!} \tag{26}$$

where

$$\ell_T = \mathrm{Max}\left\{\left|J_{\mu'} - J_\mu\right|, 1\right\} \tag{27}$$

It follows from relations (15), (24), and (26) that the Born amplitude has proportionality given by

$$\bar{f}^{B}_{m'\mu',m\mu}(\vec{q}) \propto \left(\delta_{m'm} + \frac{a_{P,\ell_P}\left|\vec{q}\right|^{\ell_P} i^{\ell_P}}{\ell_P!}\right)\left(\delta_{\mu'\mu} + \frac{a_{T,\ell_T}\left|\vec{q}\right|^{\ell_T} i^{\ell_T}}{\ell_T!}\right)\tilde{t}(k,\vec{q}) \tag{28}$$

where a_{P,ℓ_P} and a_{T,ℓ_T} are the lowest order nonvanishing transition moments of the projectile and target corresponding to equations (25) and (27).

On the basis of the Born approximation, a very strong threshold effect on the various excitation processes is observed. This effect causes an ordering in the contribution of specific excitation channels in going from small to large momentum transfer. At zero momentum transfer, only the elastic channel is open. As the momentum transfer increases, the single dipole transitions for either the target or projectile but not both are displayed first. Note that this condition severely restricts the accessible angular momentum states in the excitation process. At slightly higher momentum transfer, coincident dipole transitions in projectile and target and single quadrupole transitions are in competition with and may eventually dominate the single dipole transitions at sufficiently high momentum transfer. Similarly, at higher momentum transfer, transitions to higher angular momentum states are possible.

Perturbation Expansion and Distorted-Wave Born Approximation

According to the previous discussion, it is seen that over a restricted range of momentum transfer, the off-diagonal elements of the "Born" matrix of scattering amplitudes are small compared with the elastic scattering amplitudes for the various channels found along the diagonal. By noting that these amplitudes are proportional to the potential, a decomposition of the potential into large and small components may be made as

$$\overline{U}(\vec{x}) = \overline{U}_d(\vec{x}) + \overline{U}_0(\vec{x}) \tag{29}$$

where $\overline{U}_d(\vec{x})$ are the diagonal parts of $\overline{U}(\vec{x})$ and $\overline{U}_0(\vec{x})$ are the corresponding off-diagonal parts. It is clear that

$$\overline{U}_d(\vec{x}) >> \overline{U}_0(\vec{x}) \tag{30}$$

in accordance with the preceding discussion. Treating the off-diagonal contribution as a perturbation and considering the iterated solution will lead to substantial simplification.

Rewriting equation (7) as

$$\left[\nabla_x{}^2 + \vec{k}^2 - \overline{U}_d(\vec{x})\right]\overline{\psi}(\vec{x}) = \overline{U}_0(\vec{x})\ \overline{\psi}(\vec{x}) \tag{31}$$

and taking as a first approximation

$$\left[\nabla_x{}^2 + \vec{k}^2 - \overline{U}_d(\vec{x})\right]\overline{\psi}_0(\vec{x}) = 0 \tag{32}$$

lead to a solvable problem. The only nonzero component of $\overline{\psi}_0(\vec{x})$ is the elastic coherent scattered wave. If the initial prepared nuclei are in their ground states, then the solution for the coherent elastic wave is obtained from

$$\left(\nabla_x{}^2 + \vec{k}^2\right)\psi_c(\vec{x}) = U_{00,00}(\vec{x})\ \psi_c(\vec{x}) \tag{33}$$

and the first approximation to the coupled-channel problem is

$$\overline{\psi}_0(\vec{x}) = \begin{bmatrix} \psi_c(\vec{x}) \\ 0 \\ 0 \\ 0 \\ \cdot \\ \cdot \\ \cdot \end{bmatrix} \tag{34}$$

Estimating the perturbation by use of equation (34) yields the lowest order correction as

$$\left[\nabla_x{}^2 + \vec{k}^2 - \overline{U}_d(\vec{x})\right]\overline{\psi}^{(1)}(\vec{x}) = \overline{U}_0(\vec{x})\ \overline{\psi}_0(\vec{x}) \tag{35}$$

The right-hand side is a term describing the source of excitation caused by the interaction of the coherent amplitude and is of the form

$$\overline{U}_0(\vec{x})\ \overline{\psi}_0(\vec{x}) = \begin{bmatrix} 0 \\ U_{01,00} \\ U_{10,00} \\ U_{11,00} \\ \cdot \\ \cdot \\ \cdot \end{bmatrix}\psi_c(\vec{x}) \tag{36}$$

Since the first component of the source of excitation is zero, the equation for the first component of equation (35) is

$$\left[\nabla_x{}^2 + \vec{k}^2 - U_{00,00}(\vec{x})\right]\psi_{00}^{(1)}(\vec{x}) = 0 \tag{37}$$

and reveals that the iteration of the elastic channel yields again the coherent elastic amplitude

$$\psi_{00}^{(1)}(\vec{x}) = \psi_c(\vec{x}) \tag{38}$$

The remaining components of equation (35) are

$$\left[\nabla_x{}^2 + \vec{k}^2 - U_{m\mu,m\mu}(\vec{x})\right]\psi_{m\mu}^{(1)}(\vec{x}) = U_{m\mu,00}(\vec{x})\ \psi_c(\vec{x}) \tag{39}$$

This process of successive iteration is equivalent to the series approximation

$$\overline{\psi}(\vec{x}) = \overline{\psi}_0(\vec{x}) + \overline{\psi}_1(\vec{x}) + \overline{\psi}_2(\vec{x}) + \ . \ . \ . \tag{40}$$

where

$$\left[\nabla_x{}^2 + \vec{k}^2 - \overline{U}_d(\vec{x})\right]\overline{\psi}_0(\vec{x}) = 0 \tag{41}$$

and

$$\left[\nabla_x{}^2 + \vec{k}^2 - \overline{U}_d(\vec{x})\right]\overline{\psi}_i(\vec{x}) = \overline{U}_0(\vec{x})\ \overline{\psi}_{i-1}(\vec{x}) \tag{42}$$

The iterated solution and series solution are related as

$$\left.\begin{aligned} &\overline{\psi}_i(\vec{x}) = \overline{\psi}^{(i)}(\vec{x}) - \overline{\psi}^{(i-1)}(\vec{x}) \\ &\overline{\psi}^{(-1)}(\vec{x}) \equiv 0 \end{aligned}\right\} \tag{43}$$

and the ith iterate $\overline{\psi}^{(i)}(\vec{x})$ is the ith partial sum of the series.

Further insight can be gained by considering the formal solution to the coupled equations (41) and (42). Introducing the diagonal coherent propagator

$$G_c = \left[\nabla_x{}^2 + \vec{k}^2 - \overline{U}_d(\vec{x})\right]^{-1} \tag{44}$$

and the coherent wave operator

$$\Omega_c = 1 + \left(\nabla_x^{\,2} + \vec{k}^{\,2}\right)^{-1} \overline{U}_d(\vec{x}) \tag{45}$$

produces the solution to equation (42) as

$$\overline{\psi}_i(\vec{x}) = G_c \overline{U}_0(\vec{x})\, \overline{\psi}_{i-1}(\vec{x}) \tag{46}$$

with

$$\overline{\psi}_0 = \Omega_c \overline{\psi}_p \tag{47}$$

where $\overline{\psi}_p$ is the entering plane wave state. The series (eq. (40)) may now be written as

$$\overline{\psi} = \Omega_c \overline{\psi}_p + G_c \overline{U}_0 \Omega_c \overline{\psi}_p + G_c \overline{U}_0 G_c \overline{U}_0 \Omega_c \overline{\psi}_p + \ldots \equiv \Omega \overline{\psi}_p \tag{48}$$

The first term is the coherent elastic scattered wave as noted in equation (47) and represents attenuation and propagation of the incident plane wave in matter. Since Ω_c is diagonal, this propagation is in undisturbed matter. The second term relates to the excitation caused by the presence of the coherent elastic wave followed by coherent propagation in disturbed matter. Note that the second term has no contribution in the elastic channel. The third term relates to further excitation caused by the presence of the scattered waves formed exclusively by coherent excitation and the first correction to the elastic channel due to incoherent processes. Hence, the coherent elastic wave is correct up to second-order terms in off-diagonal elements of the potential matrix. These off-diagonal elements show considerable damping or suppression at small momentum transfer as shown in connection with equation (28). This may well be the reason why the coherent elastic amplitude has been so successful in nuclear applications. (See refs. 5 and 8.)

It is obvious from the structure of the second term in the series (eq. (48)) that it is the usual distorted-wave Born approximation (ref. 9) or single inelastic scattering approximation (ref. 10). The entire series could be aptly referred to as the distorted-wave Born series. However, if it is recalled that the terms of the series correspond to a successively larger number of changes in states of excitation (that is, the first term contains no excitation, the second term transforms the coherent elastic wave to the excited states, the third term transforms the excited states of the second term to new excitation levels and so on), a more appropriate name for the series would be the "multiple-excitation series."

Full Coupled-Channel Amplitudes

The coupled equations (7) are now solved within a small-angle approximation. This solution in effect sums the multiple-excitation series to all orders and, as a final result, gives expressions for the scattering amplitudes connecting all possible entrance channels to all possible final channels. By making the forward scattering assumption, the boundary condition is given by

$$\lim_{z \to -\infty} \bar{\psi}(\vec{x}) = \left(\frac{1}{2\pi}\right)^{3/2} \exp(i\vec{k} \cdot \vec{x})\ \bar{\delta} \tag{49}$$

where $-\hat{z}$ is the direction to the beam source and $\bar{\delta}$ is a constant vector with a unit entry at the entrance channel element and zero elsewhere. Equation (49) simply states that no particles are scattered backwards. Physically, this assumption is justified since the backward scattered component for most high-energy scattering is many orders of magnitude less than the forward scattered component. The form of the solution to equation (7) is taken as

$$\bar{\psi}(\vec{x}) = \left(\frac{1}{2\pi}\right)^{3/2} \exp\left[i\bar{\phi}(\vec{x})\right] \exp(i\vec{k} \cdot \vec{x})\ \bar{\delta} \tag{50}$$

where the boundary condition (49) implies

$$\lim_{z \to -\infty} \bar{\phi}(\vec{x}) = 0 \tag{51}$$

as a boundary condition on $\bar{\phi}(\vec{x})$. By using equation (50), one may write an equation for $\bar{\phi}(\vec{x})$ as

$$i\nabla_x^2\bar{\phi}(\vec{x}) - \left[\nabla_x\bar{\phi}(\vec{x})\right]^2 - 2\vec{k} \cdot \nabla_x\bar{\phi}(\vec{x}) - \bar{U}(\vec{x}) = 0 \tag{52}$$

If $\bar{U}(\vec{x})$ is small compared with the kinetic energy,

$$\bar{U}(\vec{x}) << k^2 \tag{53}$$

and if the change in $\bar{U}(\vec{x})$ is small over one oscillation of the incident wave, that is,

$$\nabla_x\bar{U}(\vec{x}) << \vec{k}\bar{U}(\vec{x}) \tag{54}$$

where inequalities refer to magnitudes of elements on each side of equations (53) and (54), then equation (52) may be approximated by

$$2k \frac{\partial}{\partial z} \overline{\phi}(\vec{x}) = -\overline{U}(\vec{x}) \tag{55}$$

which has the solution

$$\overline{\phi}(\vec{x}) = -\frac{1}{2k} \int_a^z \overline{U}(\vec{x}\,') \, d\vec{z}\,' \tag{56}$$

where the value a is fixed by the boundary condition (eq. (51)) to be $-\infty$. The scattered wave (eq. (50)) may now be written as

$$\overline{\psi}(\vec{x}) = \left(\frac{1}{2\pi}\right)^{3/2} \exp\left[-\frac{i}{2k} \int_{-\infty}^{z} \overline{U}(\vec{x}\,') \, d\vec{z}\,'\right] \exp(i\vec{k} \cdot \vec{x}) \, \bar{\delta} \tag{57}$$

Note that the wave operator is approximated by

$$\Omega \approx \exp\left[-\frac{i}{2k} \int_{-\infty}^{z} \overline{U}(\vec{x}\,') \, d\vec{z}\,'\right] \tag{58}$$

The eikonal result for the scattering amplitudes is given by

$$\begin{aligned} \bar{f}(\vec{q}) \, \bar{\delta} &= -\sqrt{\frac{\pi}{2}} \int \exp\left(-i\vec{k}_f \cdot \vec{x}\right) \overline{U}(\vec{x}) \, \overline{\psi}(\vec{x}) \, d^3\vec{x} \\ &= -\frac{1}{4\pi} \int \exp(-i\vec{q} \cdot \vec{x}) \, \overline{U}(\vec{x}) \exp\left[-\frac{i}{2k} \int_{-\infty}^{z} \overline{U}(\vec{x}\,') \, d\vec{z}\,'\right] \bar{\delta} \, d^3\vec{x} \end{aligned} \tag{59}$$

where $\vec{k}_f$ is the final projectile momentum and $\vec{q}$ the momentum transfer is given by

$$\vec{q} = \vec{k}_f - \vec{k} \tag{60}$$

The eikonal approximation to the coupled-channel amplitude (eq. (59)) can be further simplified by making an additional small-angle approximation as follows. By using a cylindrical coordinate system with cylinder axis along the beam direction and writing

$$\vec{x} = \vec{b} + \vec{z} \tag{61}$$

where $\vec{b}$ is the impact parameter vector, the product of $\vec{q}$ and $\vec{x}$ may be written as

$$\vec{q} \cdot \vec{x} = \vec{q} \cdot \vec{b} + O(\theta^2) \tag{62}$$

where θ is the scattering angle which is assumed to be small. This small-angle approximation allows equation (59) to be written as

$$\bar{f}(\vec{q}) = -\frac{1}{4\pi} \int \exp(-i\vec{q} \cdot \vec{b})\, \overline{U}(\vec{b} + \vec{z})\, \exp\left[-\frac{i}{2k} \int_{-\infty}^{z} \overline{U}(\vec{b} + \vec{z}\,')\, d\vec{z}\,'\right] d^2\vec{b}\, d\vec{z} \tag{63}$$

where it should be noted that the integral over $\vec{z}$ can be done exactly. Performing the integral over $\vec{z}$ in equation (63) yields the final simplified expression for the scattering amplitude as

$$\bar{f}(\vec{q}) = -\frac{ik}{2\pi} \int \exp(-i\vec{q} \cdot \vec{b}) \left\{\exp\left[i\bar{\chi}(\vec{b})\right] - 1\right\} d^2\vec{b} \tag{64}$$

where

$$\bar{\chi}(\vec{b}) = -\frac{1}{2k} \int_{-\infty}^{\infty} \overline{U}(\vec{b} + \vec{z})\, d\vec{z} \tag{65}$$

Equation (64) gives the matrix of scattering amplitudes of all possible entrance channels to all possible final channels of the system.

The relation between the eikonal result for the full scattering amplitude (eq. (64)) and the various approximate results discussed earlier in this section is now derived. First, consider the expansion in powers of $\bar{\chi}$ of the integrand of equation (64)

$$\bar{f}(\vec{q}) = -\frac{ik}{2\pi} \int \exp(-i\vec{q} \cdot \vec{b}) \left(i\bar{\chi} - \frac{1}{2}\bar{\chi}^2 - \frac{1}{3!} i\bar{\chi}^3 + \ldots\right) d^2\vec{b} \tag{66}$$

The first term is the Born approximation at small angles. Higher order terms are multiple-scattering corrections to the Born result. Recall that the Born approximation for the optical potential is equivalent to Chew's impulse approximation. A more interesting result is obtained by separating the $\bar{\chi}$ matrix into its diagonal and off-diagonal parts as

$$\bar{\chi}(\vec{b}) = \bar{\chi}_d(\vec{b}) + \bar{\chi}_0(\vec{b}) \tag{67}$$

which correspond to the diagonal and off-diagonal parts of the matrix potential $\bar{U}(\vec{x})$. An expansion in powers of the off-diagonal part of $\bar{\chi}$ in equation (64) yields

$$\bar{f}(\vec{q}) = -\frac{ik}{2\pi}\int \exp(-i\vec{q}\cdot\vec{b})\left\{\exp\left[i\bar{\chi}_d(\vec{b})\right] - 1\right\} d^2\vec{b}$$

$$-\frac{ik}{2\pi}\int \exp(-i\vec{q}\cdot\vec{b})\exp\left[i\bar{\chi}_d(\vec{b})\right]\left(i\bar{\chi}_0 - \frac{1}{2}\bar{\chi}_0^{\,2} - \frac{1}{3!}i\bar{\chi}_0^{\,3} + \ldots\right) d^2\vec{b} \tag{68}$$

The first integral is the elastic coherent amplitude, the first term of the second integral is the distorted-wave Born approximation, and the remaining terms are multiple-excitation corrections.

THE ELASTIC CHANNEL

It was shown in the previous section that within a small-angle approximation, the coupled-channel equations could be solved. The principal difficulty in calculating the full coupled-channel amplitude lies in the almost complete lack of knowledge of the internal wave functions for the colliding nuclei for all orders of excitation. It was shown on the very general principles for near forward scattering that transitions to the excited states are kinematically suppressed. This was the main motivation for expanding the solution in terms of off-diagonal matrix elements of the potential. Near forward scattering, the scattering amplitude is dominated by the diagonal elements. If elastic scattering is strongly forward, then a reasonable approximation to the elastic amplitude is obtained by neglecting the off-diagonal contribution and, in addition, the eikonal small-angle approximation should be accurate. In this vein, the elastic-channel amplitude is approximated by retaining only the first term in equation (68). Detailed comparisons with experimental data are made to justify this approximation.

It has been shown in reference 5 that the elastic-channel potential can be reduced to

$$U_c(\vec{x}) = \frac{2mA_T^{\,2}A_P^{\,2}}{N}\int d^3\vec{z}\;\rho_T(\vec{z})\int d^3\vec{y}\;\rho_P(\vec{x}+\vec{y}+\vec{z})\;\tilde{t}(k,\vec{y}) \tag{69}$$

where $\rho_T(\vec{z})$ and $\rho_P(\vec{z})$ are the target and projectile ground-state single-particle densities and $\tilde{t}(k,\vec{y})$ is the energy- and space-dependent two-body transition amplitude averaged over the projectile and target constituent types as

$$\tilde{t} = \frac{1}{A_P A_T}\left[N_P N_T t_{nn} + Z_P Z_T t_{pp} + \left(N_P Z_T + Z_P N_T\right) t_{np}\right] \tag{70}$$

N_P and N_T being the projectile and target neutron numbers and Z_P and Z_T, the corresponding proton numbers. The normalization of the $\tilde{t}$ amplitude is given by

$$\tilde{t}(k,\vec{y}) = -\frac{1}{(2\pi)^2 \mu} \int \exp(i\vec{q} \cdot \vec{y})\, f(e,\vec{q})\, d^3\vec{q} \tag{71}$$

with the usual expression for the spin-independent two-nucleon transition amplitudes as

$$f(e,\vec{q}) = \frac{\sqrt{me}\,\sigma(e)}{4\pi}\left[\alpha(e) + i\right] \exp\left[-\frac{1}{2} B(e)\, \vec{q}^{\,2}\right] \tag{72}$$

where e is the constituent energy in the two-body center-of-mass frame, $\mu = m/2$ is the two-body reduced mass, $\sigma(e)$ is the energy-dependent total two-body cross section, $\alpha(e)$ is the ratio of real to imaginary parts, and $B(e)$ is the slope parameter. The elastic-channel phase function may now be approximated by

$$\chi(\vec{b}) = -\frac{1}{2k}\int_{-\infty}^{\infty} U_c(\vec{b} + \vec{z})\, d\vec{z} \tag{73}$$

from which the elastic-channel amplitude may be calculated by

$$f_c(\vec{q}) = -ik \int_0^{\infty} b\, db\, J_0\left(2kb \sin\frac{\theta}{2}\right)\left\{\exp\left[i\chi(\vec{b})\right] - 1\right\} \tag{74}$$

where the property that the phase function is cylindrically symmetric about the $\hat{z}$-direction has been used. Applying now the optical theorem

$$\sigma_{tot} = \frac{4\pi}{k}\, \mathrm{Im}\left[f_c(\vec{0})\right] \tag{75}$$

yields

$$\sigma_{tot} \approx 4\pi \int_0^{\infty} b\, db \left\{1 - \exp\left[-\chi_i(\vec{b})\right] \cos\left[\chi_r(\vec{b})\right]\right\} \tag{76}$$

where χ_r and χ_i are the real and imaginary parts of χ. Since the scattering is strongly forward, the total elastic cross section may be calculated by using the eikonal expression by

$$\sigma_s = \int \left|f(\vec{q})\right|^2 d\hat{q}$$

$$\approx 4\pi \int_0^\infty b\ db \left\{1 - \exp\left[-\chi_i(\vec{b})\right] \cos\left[\chi_r(\vec{b})\right]\right\} - 2\pi \int_0^\infty b\ db \left\{1 - \exp\left[-2\chi_i(\vec{b})\right]\right\} \tag{77}$$

from which it follows that

$$\sigma_{abs} = \sigma_{tot} - \sigma_s \approx 2\pi \int_0^\infty b\ db \left\{1 - \exp\left[-2\chi_i(\vec{b})\right]\right\} \tag{78}$$

The use of approximations (76) to (78) has at least in part been justified by comparison with experiment. (See ref. 5.) The following is an attempt to quantify the accuracy of these approximations by further comparison with experiments.

THE PHYSICAL DATA

It was noted in the previous section that scattering in the elastic channel can be described in terms of the single-particle density functions of the projectile and target and the nucleon-nucleon two-body transition amplitudes. For the present work, these functions are determined from compilations of experimental results on electron scattering from nuclei (that is, nuclear charge distributions) and nucleon-nucleon scattering experiments.

Single-Particle Density

The single-particle densities are related to the nuclear wave functions by

$$\rho_A(\vec{r}) = \frac{1}{A} \sum_{i=1}^{A} \left\langle g_0(\vec{\xi}) \middle| \delta\left(\vec{r} - \vec{r}_i\right) \middle| g_0(\vec{\xi}) \right\rangle \tag{79}$$

which can be written as

$$\rho_A(\vec{r}) = \frac{1}{A}\left[N_A \rho_n(\vec{r}) + Z_A \rho_p(\vec{r})\right] \tag{80}$$

where $\rho_n(\vec{r})$ and $\rho_p(\vec{r})$ are the corresponding neutron and proton densities. It can be assumed for light nuclei that

$$\rho_n(\vec{r}) \approx \rho_p(\vec{r}) \tag{81}$$

since they differ only by the coulomb repulsion of the protons which is a small effect in light nuclei. The medium mass nuclei would probably satisfy the relation

$$\int \vec{r}^{\,2}\rho_p(\vec{r})\, d^3\vec{r} > \int \vec{r}^{\,2}\rho_n(\vec{r})\, d^3\vec{r} \tag{82}$$

strictly as a result of coulomb repulsion. The inequality (82) may actually be reversed in very heavy nuclei because of the large neutron excesses and the fact that the nuclear binding of the protons is greatly increased because of this excess. For example, the charge radius has been observed to be relatively reduced in isotopes with increasing neutron numbers. (See ref. 11.) In the present work, it is assumed that

$$\rho_n(\vec{r}) = \rho_p(\vec{r}) \tag{83}$$

and the proton densities are taken from electron scattering experiments.

Electron scattering experiments measure the charge distribution of the nucleus. Had the proton been a point particle, then the charge and proton densities would be proportional. The structure of the proton requires one to extract the single-particle (or proton) densities by removing the effects of the proton charge distribution.

The single-particle density (eq. (80)) is then related to the charge distribution as measured by electron scattering through the following expression:

$$\rho_{C,A}(\vec{r}) = \int \rho_{C,p}(\vec{r}\,')\, \rho_A(\vec{r} + \vec{r}\,')\, d^3\vec{r}\,' \tag{84}$$

where $\rho_{C,p}(\vec{r})$ is the charge distribution of the proton and $\rho_{C,A}(\vec{r})$ is the nuclear-charge density. One must now solve the integral equation (84) for the nuclear single-particle density $\rho_A(\vec{r})$.

The proton charge form factor is, to a good approximation, a gaussian function (ref. 12) as

$$\rho_{C,p}(\vec{r}) = \left(\frac{3}{2\pi a_p^2}\right)^{3/2} \exp\left(\frac{-3\vec{r}^{\,2}}{2a_p^2}\right) \tag{85}$$

with $a_p \approx 0.8$ fm. Substituting equation (85) into equation (84) and simplifying yields

$$\rho_{C,A}(\vec{r}) = \left(\frac{2\pi a_p{}^2}{3}\right)^{-1/2} \left\{ \frac{a_p{}^2}{3r} \int_0^\infty \exp(-s) \left[\rho_A\left(r - \sqrt{\frac{2a_p{}^2 s}{3}}\right) - \rho_A\left(r + \sqrt{\frac{2a_p{}^2 s}{3}}\right)\right] ds \right.$$

$$\left. + \sqrt{\frac{2a_p{}^2}{3}} \int_{-\infty}^{\infty} \exp(-s^2)\, \rho_A\left(r + \sqrt{\frac{2a_p{}^2}{3}}\, s\right) ds \right\} \tag{86}$$

The first term in equation (86) contributes only when r is near the nuclear edge. Its importance at the nuclear edge is estimated by assuming the worst case when $\rho_A(\vec{r})$ is a uniform model density and r is taken to be the equivalent uniform radius r_u. The two terms in equation (86) at $r = r_u$ are written as

$$\rho_{C,A}(\vec{r}) \approx \frac{1}{\sqrt{6\pi}} \frac{a_p}{r_u} \rho_0 + \frac{1}{\sqrt{\pi}} \int_{-\sqrt{\frac{3}{2a_p{}^2}}\, r_u}^{0} \exp(-s^2)\, \rho_0\, ds \approx \frac{1}{\sqrt{6\pi}} \frac{a_p}{r_u} \rho_0 + \frac{1}{2} \rho_0 \tag{87}$$

where ρ_0 is the central density. Comparing the ratio of the first term with the second as

$$\left(\frac{2}{3\pi}\right)^{1/2} \frac{a_p}{r_u} \approx \frac{0.36}{r_u} \leqq 0.15 \tag{88}$$

with $r_u \geqq 2.4$ fm. Hence, the first term is less than or on the order of 15 percent. As a further test of the importance of the first term, numerical experiments were performed for the typical Woods-Saxon density and the first term was found to be less than 1 percent of the second. The first term is therefore neglected as

$$\rho_{C,A}(\vec{r}) = \frac{1}{\sqrt{\pi}} \int_{-\infty}^{\infty} \exp(-s^2)\, \rho_A\left(r + \sqrt{\frac{2a_p{}^2}{3}}\, s\right) ds \tag{89}$$

Use of the two-point Gauss-Hermite quadrature formula yields

$$\rho_{C,A}(\vec{r}) \approx \frac{1}{2}\left[\rho_A\left(\frac{r + a_p}{\sqrt{3}}\right) + \rho_A\left(\frac{r - a_p}{\sqrt{3}}\right)\right] \tag{90}$$

which is equivalent to assuming that $\rho_A(r)$ is well approximated by a cubic over the range of $r \pm a_p$ (ref. 13). The formula (90) was shown to be accurate within 2 percent as determined by numerical evaluation of equation (86).

In the present work the densities of nuclei heavier than helium are assumed to be approximately Woods-Saxon in shape as given by

$$\rho(r) = \left[1 + \exp\left(\frac{r - R}{a}\right)\right]^{-1} \tag{91}$$

except for an overall normalization factor. In equation (91), R is the radius at half density

$$R = r_{0.5} \tag{92}$$

and a is related to the skin thickness t by

$$t = 4.4a \tag{93}$$

Values for the half-density radius and skin thickness determined from electron scattering experiments have been compiled by Hofstadter and Collard (ref. 12) and are shown in figures 1 and 2.

It was found on the basis of equation (89) that the half-density radius of the charge distribution was equal to the half-density radius of the single-particle densities. Hence, the half-density radius for $\rho_A(\vec{r})$ may be taken directly from the compilations of reference 12. The single-particle skin thickness is yet to be determined from approximation (90). Except for the overall normalization, equation (90) evaluated at $r = \frac{R + a_p}{\sqrt{3}}$ results in

$$a = \frac{\frac{2}{\sqrt{3}} a_p}{\log_e\left(\frac{3z - 1}{3 - z}\right)} \tag{94}$$

where

$$z = \exp\left(\frac{a_p}{\sqrt{3}\, a_C}\right) \tag{95}$$

with a_C as the charge density parameter and a as the single-particle density parameter. Equations (94) and (95) were used to determine the single-particle skin thickness

$$t = 4.4a \tag{96}$$

in terms of the charge skin thickness

$$t_C = 4.4a_C \tag{97}$$

and the proton root-mean-square (rms) charge radius a_p given by

$$a_p{}^2 = \int \vec{r}^{\,2} \rho_{C,p}(\vec{r})\, d^3\vec{r} \tag{98}$$

The charge skin thickness and proton rms radius are taken from reference 12. The nuclear single-particle density skin thickness as determined from the nuclear charge skin thickness is shown in figure 3. The skin thicknesses calculated by using equations (94) to (98) were shown to satisfy equation (86) to within 1 percent.

For the purposes of the present calculations, the relation

$$r_{0.5} = 1.18A^{1/3} - 0.48 \tag{99}$$

was used to obtain the half-density radius (fm). Values for the single-particle skin thickness were obtained by spline interpolation between the values given in table 1. The experimental deviations from equation (99) and interpolated values from table 1 are given in table 2 for several common elements used in scattering experiments.

Nucleon-Nucleon Scattering Amplitude

The two-body amplitudes required for the present calculations are the proton-proton and proton-neutron scattering amplitudes. In the present work, the coulomb scattering contribution is neglected and use is made of the following form:

$$f_i(e,\vec{q}) = \frac{\sqrt{me}}{4\pi}\, \sigma_i(e)\left[\alpha_i(e) + i\right] \exp\left[-\frac{1}{2} B_i(e)\, \vec{q}^{\,2}\right] \tag{100}$$

for $i = np,pp$. The parameters σ_i, α_i, and B_i were taken from the compilations of references 14 and 15. Graphs of these functions as estimated from references 14 and 15 are shown in figures 4 to 9 where the values are shown by dots at discrete energies and the range of experimental uncertainty is indicated by the two curves. The deviations of experimental values from the average values given by

$$\sigma(e) = \frac{1}{2}\left[\sigma_{pp}(e) + \sigma_{np}(e)\right] \tag{101}$$

$$\alpha(e) = \frac{\sigma_{pp}(e)\,\alpha_{pp}(e) + \sigma_{np}(e)\,\alpha_{np}(e)}{\sigma_{pp}(e) + \sigma_{np}(e)} \tag{102}$$

$$B(e) = \frac{1}{2}\left[B_{pp}(e) + B_{np}(e)\right] \tag{103}$$

are given in table 3. The uncertainties in table 3 are used to estimate uncertainty in the present calculations although in the calculations the average two-body amplitude is calculated essentially from equation (70) which deviates slightly from equations (101) and (102). Equation (103) is used to estimate the average slope parameter for convenience and the error introduced is negligible since this parameter contributes only a few percent to the nuclear cross sections for energies less than 30 GeV.

NUCLEON-NUCLEUS SCATTERING

The case of nucleon-nucleus scattering is considered first since a large body of experimental data is available with which to make comparisons. Attention is given to the targets of carbon, aluminum, copper, and lead since for these targets the data are most complete. The experimental cross sections are taken from the compilations of Barashenkov et al. (ref. 16) and the experiments of Schimmerling et al. (refs. 17 and 18).

The neutron-nucleus scattering cross sections were calculated by using the eikonal and coherent approximations discussed previously. The physical data required for the calculations are discussed in the previous section. By using equations (76) and (78), the total and absorption cross sections were calculated for the four aforementioned targets and the comparisons of the calculations with the experimental results are shown in figures 10 to 17. The uncertainty in the theoretical results due to uncertainty in the input physical data is indicated by the two curves. These uncertainties in cross sections were estimated by determining the effect of uncertainty in each input parameter separately and using the rms value of each effect to obtain the total uncertainty. This process was performed at each of the five energies shown in table 3 with the results for each of the four targets in table 4. The curves were obtained by linear interpolation of the values in table 4. The points between the curves are the cross-sectional values calculated at the indicated energies.

Generally, the agreement between the present calculations and experiment is very good, the largest errors being about 15 percent which occurs below 300 MeV. This error is suspected to be in part due to the eikonal approximation. For example, the eikonal approximation requires the contribution of a large number of partial waves. Note, however, that even in lead the angular momentum is

$$\ell \approx kR_{Pb} = 12 \tag{104}$$

and leads one to anticipate large corrections to the eikonal result. Above 300 MeV, the largest error is for carbon total cross section with differences on the order of 5 percent. There is a real disagreement for aluminum total cross sections above 300 MeV of a few percent whereas copper and lead agree within the theoretical and experimental uncertainty. These errors may result from the effective potential approximation which tends to overestimate shadow effects.

The results for absorption cross sections show much better agreement with the experimental results. This difference, of course, is in part due to the greater scatter in the experimental values. Even so, it appears that the absorption cross section is more accurately predicted than the elastic cross section. This is especially true below 300 MeV.

The results of comparison with experiments are that the coherent approximation to the elastic channel appears to be reasonable and that the eikonal approximation to the coherent amplitude is good above 300 MeV for nucleon-nucleus scattering. Below 300 MeV, it is expected that because of the small number of contributing partial waves, the eikonal approximation results in an error which is never more than about 15 percent.

The nucleon-nucleus cross sections are given as a function of energy in tables 5 to 8.

NUCLEUS-NUCLEUS SCATTERING

On the basis of the approximations discussed in previous sections, total and absorption cross sections for selected heavy ions with various target nuclei have been calculated and the results are given in tables 9 to 32. An attempt has been made to include projectiles which are likely to be available at heavy-ion accelerators and common target materials. At the same time, most of the data of interest to cosmic-ray shielding is either contained in the tables or can be obtained by interpolation in nuclear mass number. Although it is difficult to affix an error to the tables at the present time, the error may surely be regarded as no worse than about 10 percent since the largest errors anticipated are due to the eikonal approximation which is most accurate for heavy-ion collisions. A more accurate assessment must await new experimental results.

CONCLUDING REMARKS

The solution of the coupled-channel equation for heavy-ion reaction has been obtained. Approximation of the elastic amplitude by neglecting terms related to internal excitation and terms higher than second order in scattering angle was found to be accurate. On this basis, the total and absorption cross sections were calculated for the scattering of nucleons from nuclei. Comparison with experimental results indicates errors are within 5 percent for energies above 300 MeV; the errors are within 15 percent for energies between 100 and 300 MeV. The 15-percent errors at low energy are believed to be due to the eikonal approximation. Tables of heavy-ion cross sections were calculated for use in cosmic-ray transport studies. The eikonal approximation for heavy-ion scattering is believed to be adequate because of the larger number of contributing partial waves even at 100 MeV.

Langley Research Center
National Aeronautics and Space Administration
Hampton, Va. 23665
November 28, 1975

REFERENCES

1. Schaefer, Hermann J.: Public Health Aspects of Galactic Radiation Exposure at Supersonic Transport Altitudes. Aerosp. Medicine, vol. 39, no. 12, Dec. 1968, pp. 1298-1303.

2. Langham, Wright H., ed.: Radiobiological Factors in Manned Space Flight. Publ. 1487, Natl. Acad. Sci. – Natl. Res. Counc., 1967.

3. Curtis, S. B.; and Wilkinson, M. C.: The Heavy Particle Hazard – What Physical Data are Needed? Proceedings of the National Symposium on Natural and Manmade Radiation in Space, E. A. Warman, ed., NASA TM X-2440, 1972, pp. 1007-1015.

4. Wilson, J. W.: Multiple Scattering of Heavy Ions, Glauber Theory, and Optical Model. Phys. Lett., vol. B52, no. 2, Sept. 1974, pp. 149-152.

5. Wilson, John W.: Composite Particle Reaction Theory. Ph. D. Diss., The College of William and Mary in Virginia, June 1975.

6. Chew, Geoffrey F.: High Energy Elastic Proton-Deuteron Scattering. Phys. Rev., Second ser., vol. 84, no. 5, Dec. 1951, pp. 1057-1058.

7. Watson, Kenneth M.: Multiple Scattering and the Many-Body Problem – Applications to Photomeson Production in Complex Nuclei. Phys. Rev., Second ser., vol. 89, no. 3, Feb. 1953, pp. 575-587.

8. Best, Melvyn E.: Particle-Nucleus Scattering at Intermediate Energies. Canadian J. Phys., vol. 50, no. 14, July 1972, pp. 1609-1613.

9. Austern, N.: Direct Reaction Theories. Fast Neutron Physics. Part II: Experiments and Theory, J. B. Marion and J. L. Fowler, eds., Interscience Publ., 1963, pp. 1113-1216.

10. Goldberger, Marvin L.; and Watson, Kenneth M.: Collision Theory. John Wiley & Sons, Inc., c.1964.

11. Bohr, Aage; and Mottelson, Ben R.: Nuclear Structure. Volume I – Single Particle Motion, W. A. Benjamin, Inc., 1969.

12. Hofstadter, R.; and Collard, H. R.: Nuclear Radii Determined by Electron Scattering. Landolt-Börnstein Numerical Data and Functional Relationships in Science and Technology, Group I, Vol. 2, H. Schopper, ed., Springer-Verlag, 1967, pp. 21-52.

13. Krylov, Vladimir Ivanovich (Arthur H. Stroud, trans.): Approximate Calculation of Integrals. Macmillan Co., c.1962.

14. Hellwege, K. -H., ed.: Elastische und Ladungsaustausch-Streuung von Elementarteilchen. Landolt-Bornstein Numerical Data and Functional Relationships in Science and Technology, Group I, Vol. 7, Springer-Verlag, 1973.

15. Benary, Odette; Price, Leroy R.; and Alexander, Gideon: NN and ND Interactions (Above 0.5 GeV/c) – A Compilation. UCRL-20000 NN, Lawrence Radiation Lab., Univ. California, Aug. 1970.

16. Barashenkov, V. S.; Gudima, K. K.; and Toneev, V. D.: Cross Sections for Fast Particles and Atomic Nuclei. Progress of Phys., vol. 17, no. 10, 1969, pp. 683-725.

17. Schimmerling, W.; Devlin, T. J.; Johnson, W.; Vosburgh, K. G.; and Mischke, R. E.: Neutron-Nucleus Total Cross Sections From 900 to 2600 MeV/c. Phys. Lett., vol. 37B, no. 2, Nov. 1971, pp. 177-180.

18. Schimmerling, Walter; Devlin, Thomas J.; Johnson, Warren W.; Vosburgh, Kirby G.; and Mischke, Richard E.: Neutron-Nucleus Total and Inelastic Cross Sections: 900 to 2600 MeV/c. Phys. Rev. C, Third ser., vol. 7, no. 1, Jan. 1973, pp. 248-262.

TABLE 1.- NUCLEAR SKIN THICKNESS

$A^{1/3}$	t, fm	$A^{1/3}$	t, fm
1.75	1.81	3.46	2.16
2.02	1.75	3.71	1.90
2.19	1.51	3.90	1.69
2.38	1.19	4.13	1.53
2.46	1.01	4.43	1.67
2.66	.90	4.73	1.77
2.83	1.08	5.11	1.83
2.94	1.44	5.50	1.80
3.03	1.78	5.86	1.77
3.22	2.06	6.00	1.75

TABLE 2.- PERCENTAGE UNCERTAINTY IN NUCLEON DENSITY PARAMETERS

Target nucleus	Percentage uncertainty for –	
	Half-radius, $r_{0.5}$	Skin thickness, t
C	2.7	2.6
Al	3.3	4.6
Cu	3.2	7.8
Pb	3.1	10.9

TABLE 3.- PERCENTAGE UNCERTAINTY IN NUCLEON-NUCLEON COLLISION PARAMETERS

Incident energy, GeV/amu	Percentage uncertainty for –		
	Re(f)/Im(f), α	Nucleon-nucleon cross section, σ	Slope parameter, B
0.1	47	3.4	7.8
.5	53	3.1	7.1
1.0	67	.9	6.3
5.0	35	2.7	5.1
10.0	33	2.1	6.1

TABLE 4.- PERCENTAGE UNCERTAINTY IN NEUTRON-NUCLEUS CROSS SECTIONS

Incident energy, GeV/amu	Percentage uncertainty for –			
	C	Al	Cu	Pb
0.1	1.8	2.9	4.2	5.0
.5	1.3	2.0	3.0	4.0
1.0	1.4	2.3	3.3	4.3
5.0	1.3	2.1	3.2	4.2
10.0	1.4	2.1	3.1	4.1

TABLE 5.- NEUTRON-NUCLEUS TOTAL CROSS SECTION

Energy, MeV/amu	Neutron-nucleus total cross section, mb, for –									
	He	C	O	Al	A	Fe	Br	Ag	Ba	Pb
100	178	428	496	805	1128	1349	1670	2094	2457	3215
125	163	401	474	767	1075	1308	1633	2051	2413	3170
150	155	384	459	744	1046	1283	1610	2027	2388	3147
175	142	355	429	697	984	1221	1549	1959	2319	3079
200	128	321	391	636	903	1132	1453	1849	2203	2957
225	120	303	369	602	857	1080	1395	1780	2128	2875
250	115	289	353	576	821	1038	1346	1722	2065	2803
275	111	278	339	555	792	1003	1304	1671	2008	2735
300	108	271	332	542	775	981	1278	1639	1972	2692
350	107	267	325	533	763	964	1257	1612	1941	2653
400	108	268	326	534	764	962	1253	1606	1934	2641
500	118	289	348	570	817	1016	1315	1679	2018	2736
600	128	309	369	605	857	1068	1374	1749	2097	2827
700	133	321	381	624	894	1095	1404	1784	2136	2870
800	138	330	390	639	914	1116	1427	1811	2165	2903
900	141	337	398	651	930	1133	1446	1833	2188	2929
1000	144	342	404	659	941	1145	1459	1849	2206	2948
1250	148	350	413	673	958	1166	1482	1875	2233	2979
1500	150	355	419	680	966	1176	1493	1889	2248	2996
1750	152	358	423	685	972	1183	1502	1899	2259	3009
2000	154	360	426	689	977	1190	1510	1908	2269	3021
2500	154	361	428	691	978	1193	1514	1913	2274	3027
3000	154	360	427	688	974	1189	1511	1909	2269	3023
3500	153	358	425	685	969	1185	1507	1904	2264	3018
4000	152	356	423	681	965	1181	1502	1898	2258	3011
5000	151	353	420	678	950	1175	1496	1892	2251	3004
6000	150	351	417	673	954	1169	1489	1884	2243	2995
7000	148	348	414	668	947	1161	1481	1873	2231	2982
8000	147	346	412	664	941	1155	1473	1865	2222	2971
9000	147	344	410	661	937	1150	1469	1859	2215	2964
10000	147	343	409	659	934	1147	1465	1855	2211	2959
12500	147	342	408	656	930	1142	1460	1848	2204	2952
15000	146	340	406	653	924	1137	1454	1841	2196	2943
17500	146	338	404	649	919	1131	1447	1833	2187	2933
20000	145	337	403	645	913	1125	1441	1825	2179	2923
22500	145	336	402	643	910	1122	1437	1820	2173	2916

TABLE 6.- NEUTRON-NUCLEUS ABSORPTION CROSS SECTION

Energy, MeV/amu	Neutron-nucleus absorption cross section, mb, for –									
	He	C	O	Al	A	Fe	Br	Ag	Ba	Pb
100	111	246	271	447	629	726	884	1107	1295	1680
125	102	230	257	422	593	694	851	1067	1252	1633
150	97	222	249	409	577	678	835	1049	1233	1612
175	93	214	242	398	561	663	820	1031	1213	1592
200	90	208	237	388	548	650	807	1015	1197	1574
225	87	203	232	380	537	639	796	1002	1183	1559
250	85	199	228	374	529	632	788	993	1173	1548
275	84	197	226	370	524	627	783	987	1167	1542
300	84	196	225	369	522	625	781	985	1165	1540
350	84	196	225	369	523	626	783	987	1168	1543
400	85	198	228	373	529	631	789	995	1177	1553
500	92	211	241	395	560	661	822	1033	1221	1603
600	99	223	252	413	587	686	849	1065	1257	1643
700	102	230	258	423	601	699	863	1082	1275	1664
800	105	234	262	430	611	709	873	1093	1288	1678
900	107	238	265	436	618	715	880	1102	1297	1688
1000	108	240	268	439	622	720	885	1107	1303	1694
1250	110	243	271	443	626	724	890	1112	1308	1700
1500	111	244	273	444	628	726	892	1114	1310	1703
1750	112	246	274	446	629	728	894	1117	1313	1705
2000	113	246	275	447	630	729	895	1118	1314	1707
2500	113	247	276	447	629	729	895	1117	1313	1706
3000	113	246	275	445	626	727	893	1115	1310	1703
3500	112	245	274	443	624	725	891	1112	1307	1700
4000	112	244	274	442	622	723	890	1111	1306	1699
5000	111	243	273	441	621	722	889	1110	1305	1698
6000	111	242	272	440	619	720	887	1108	1303	1696
7000	110	241	271	438	617	718	885	1105	1300	1692
8000	110	241	271	437	615	717	883	1103	1298	1690
9000	110	240	271	437	614	717	883	1103	1298	1690
10000	110	241	271	437	615	717	884	1103	1298	1691
12500	111	241	272	438	615	718	885	1105	1300	1693
15000	111	241	273	438	614	718	886	1105	1300	1694
17500	111	241	273	437	613	717	885	1104	1299	1693
20000	111	241	273	437	612	716	885	1104	1298	1692
22500	111	241	273	437	612	716	885	1104	1299	1693

TABLE 7.- PROTON-NUCLEUS TOTAL CROSS SECTION

Energy, MeV/amu	Proton-nucleus total cross section, mb, for –									
	He	C	O	Al	A	Fe	Br	Ag	Ba	Pb
100	178	428	496	817	1171	1377	1716	2148	2540	3319
125	163	401	474	780	1122	1337	1681	2106	2494	3267
150	155	384	459	756	1088	1310	1656	2078	2464	3234
175	142	355	429	707	1020	1246	1592	2008	2390	3160
200	128	321	391	644	931	1151	1488	1889	2263	3028
225	120	303	369	609	880	1097	1425	1816	2182	2940
250	115	289	353	581	841	1052	1373	1753	2111	2859
275	111	278	339	559	808	1014	1325	1696	2045	2779
300	108	271	332	546	789	991	1295	1659	2002	2727
350	107	267	326	536	773	971	1269	1626	1963	2677
400	108	268	326	536	772	967	1262	1616	1949	2658
500	118	289	348	569	816	1014	1311	1673	2008	2721
600	128	309	369	603	861	1062	1363	1734	2074	2795
700	133	321	381	622	885	1089	1393	1770	2114	2840
800	138	330	390	637	907	1111	1417	1799	2146	2878
900	141	337	398	649	923	1128	1437	1822	2173	2909
1000	144	342	404	658	936	1142	1453	1841	2194	2934
1250	148	350	413	673	957	1165	1482	1875	2234	2981
1500	150	355	419	680	967	1177	1496	1893	2254	3006
1750	152	358	423	685	973	1185	1506	1904	2267	3020
2000	154	360	426	690	979	1192	1515	1914	2278	3034
2500	154	361	428	691	981	1196	1520	1920	2285	3043
3000	154	360	427	689	978	1193	1518	1918	2283	3041
3500	153	358	425	686	974	1189	1514	1913	2278	3036
4000	152	356	423	682	969	1184	1508	1906	2270	3027
5000	151	353	420	678	962	1177	1499	1896	2258	3014
6000	150	351	417	674	956	1170	1492	1887	2249	3002
7000	148	348	414	668	949	1163	1484	1877	2238	2990
8000	147	346	412	664	943	1156	1476	1869	2228	2979
9000	147	344	410	661	939	1152	1471	1862	2221	2970
10000	147	343	409	659	935	1148	1466	1857	2214	2963
12500	147	342	408	656	929	1142	1459	1847	2202	2949
15000	146	340	406	652	923	1136	1452	1839	2193	2938
17500	146	338	404	648	917	1130	1445	1830	2183	2928
20000	145	337	403	645	912	1124	1439	1823	2175	2918
22500	145	336	402	643	909	1121	1435	1818	2170	2912

TABLE 8.- PROTON-NUCLEUS ABSORPTION CROSS SECTION

Energy, MeV/amu	Proton-nucleus absorption cross section, mb, for –									
	He	C	O	Al	A	Fe	Br	Ag	Ba	Pb
100	111	246	271	452	647	738	905	1133	1336	1731
125	102	230	257	426	611	705	872	1093	1292	1684
150	97	222	249	414	593	688	854	1072	1268	1658
175	93	214	242	401	575	672	837	1052	1246	1633
200	90	208	237	391	561	659	823	1035	1227	1612
225	87	203	232	383	549	648	811	1022	1212	1596
250	85	199	228	377	540	640	803	1011	1201	1583
275	84	197	226	373	535	634	797	1004	1193	1574
300	84	196	225	371	531	631	793	1000	1188	1569
350	84	196	225	371	531	631	793	999	1187	1567
400	85	198	228	375	536	636	798	1005	1192	1573
500	92	211	241	395	562	662	824	1035	1224	1607
600	99	223	252	413	585	685	847	1062	1252	1637
700	102	230	258	423	598	697	859	1077	1268	1654
800	105	234	262	429	607	706	868	1087	1279	1667
900	107	238	265	434	614	713	875	1095	1288	1676
1000	108	240	268	438	618	717	880	1101	1294	1683
1250	110	243	271	442	624	723	887	1108	1302	1693
1500	111	244	273	444	626	725	890	1112	1307	1698
1750	112	246	274	446	628	727	893	1115	1310	1702
2000	113	246	275	447	629	729	894	1117	1312	1704
2500	113	247	276	447	628	729	895	1117	1313	1706
3000	113	246	275	445	626	727	893	1115	1311	1704
3500	112	245	274	444	624	725	891	1113	1308	1701
4000	112	244	274	442	622	723	890	1111	1306	1698
5000	111	243	273	441	620	722	887	1108	1303	1695
6000	111	242	272	440	618	720	885	1106	1300	1692
7000	110	241	271	438	616	718	883	1103	1297	1689
8000	110	241	271	437	614	716	882	1102	1295	1687
9000	110	240	271	437	614	716	882	1101	1295	1686
10000	110	241	271	437	614	716	882	1101	1295	1686
12500	111	241	272	437	614	716	882	1102	1295	1687
15000	111	241	273	437	613	716	883	1102	1296	1688
17500	111	241	273	437	612	716	883	1102	1295	1687
20000	111	241	273	436	611	715	882	1101	1294	1687
22500	111	241	273	436	611	715	882	1101	1294	1687

TABLE 9.- HELIUM-NUCLEUS TOTAL CROSS SECTION

Energy, MeV/amu	Helium-nucleus total cross section, mb, for –									
	He	C	O	Al	A	Fe	Br	Ag	Ba	Pb
100	466	880	953	1432	1938	2154	2544	3092	3557	4462
125	442	848	924	1389	1881	2101	2491	3030	3491	4390
150	428	830	907	1365	1849	2072	2461	2995	3453	4349
175	403	797	876	1321	1791	2016	2404	2930	3382	4272
200	372	753	834	1262	1714	1943	2327	2842	3287	4168
225	353	727	809	1226	1669	1899	2282	2790	3231	4106
250	339	705	788	1197	1631	1863	2244	2747	3184	4055
275	327	686	770	1171	1598	1831	2210	2708	3142	4009
300	320	674	759	1155	1577	1810	2189	2684	3116	3980
350	315	665	749	1141	1559	1793	2171	2663	3093	3955
400	315	663	747	1139	1556	1790	2167	2659	3089	3950
500	336	693	775	1178	1607	1838	2217	2716	3151	4018
600	357	723	804	1218	1658	1888	2269	2776	3215	4088
700	368	739	820	1240	1687	1916	2298	2809	3251	4127
800	377	752	833	1258	1710	1938	2321	2835	3279	4159
900	384	763	843	1272	1728	1955	2339	2856	3302	4184
1000	390	771	851	1283	1741	1969	2354	2872	3319	4203
1250	399	785	865	1301	1764	1992	2378	2900	3349	4236
1500	404	792	873	1311	1776	2004	2392	2915	3365	4254
1750	407	798	879	1318	1784	2013	2402	2926	3377	4268
2000	410	802	884	1325	1791	2021	2410	2935	3387	4279
2500	412	805	888	1328	1795	2026	2416	2941	3394	4287
3000	411	804	887	1327	1792	2024	2414	2939	3391	4285
3500	409	802	885	1324	1789	2021	2411	2935	3387	4280
4000	408	800	883	1321	1784	2016	2407	2930	3382	4274
5000	405	796	880	1316	1778	2011	2401	2924	3375	4266
6000	403	793	876	1311	1772	2005	2395	2917	3367	4258
7000	400	788	872	1306	1765	1998	2388	2908	3358	4248
8000	398	785	869	1301	1759	1992	2382	2902	3351	4241
9000	396	783	868	1299	1755	1989	2379	2898	3347	4236
10000	396	782	867	1297	1753	1987	2377	2896	3345	4234
12500	395	781	866	1295	1749	1985	2375	2893	3342	4231
15000	394	780	866	1293	1746	1982	2373	2891	3339	4228
17500	392	777	864	1290	1741	1979	2370	2886	3334	4224
20000	391	775	863	1287	1737	1975	2366	2883	3330	4219
22500	390	774	862	1286	1735	1973	2365	2881	3328	4217

TABLE 10.- HELIUM-NUCLEUS ABSORPTION CROSS SECTION

Energy, MeV/amu	Helium-nucleus absorption cross section, mb, for –									
	He	C	O	Al	A	Fe	Br	Ag	Ba	Pb
100	269	487	519	778	1054	1153	1348	1635	1875	2335
125	252	464	498	747	1013	1115	1310	1590	1827	2283
150	244	453	487	733	993	1097	1291	1569	1804	2257
175	236	443	478	719	975	1080	1274	1549	1781	2234
200	230	434	470	707	959	1066	1259	1532	1763	2214
225	225	427	464	698	947	1054	1248	1519	1749	2198
250	221	422	459	691	938	1046	1239	1509	1738	2186
275	219	419	456	687	932	1041	1234	1502	1731	2179
300	218	418	455	685	930	1038	1231	1499	1728	2176
350	218	418	455	686	930	1039	1232	1500	1729	2177
400	221	422	458	690	936	1045	1238	1507	1736	2185
500	234	440	476	714	968	1075	1269	1543	1775	2226
600	246	456	491	736	996	1101	1296	1574	1808	2263
700	252	465	499	748	1011	1116	1311	1591	1827	2284
800	257	471	505	756	1022	1126	1322	1603	1840	2298
900	260	476	510	762	1030	1134	1329	1612	1850	2309
1000	263	479	513	766	1036	1139	1335	1619	1857	2316
1250	266	483	517	772	1042	1145	1342	1626	1865	2325
1500	267	485	520	774	1045	1149	1346	1630	1869	2330
1750	269	487	522	777	1047	1151	1349	1633	1873	2334
2000	270	488	523	778	1048	1153	1351	1636	1875	2337
2500	270	489	524	778	1048	1153	1351	1636	1876	2338
3000	269	488	523	777	1046	1152	1350	1634	1873	2335
3500	268	487	522	775	1043	1150	1348	1632	1871	2333
4000	267	486	521	774	1042	1148	1346	1630	1869	2331
5000	267	485	521	773	1040	1146	1345	1628	1867	2328
6000	266	483	519	771	1038	1144	1343	1625	1864	2325
7000	265	482	518	769	1035	1142	1340	1623	1861	2322
8000	264	481	517	768	1033	1141	1339	1621	1859	2320
9000	264	481	517	768	1033	1141	1339	1621	1859	2320
10000	264	481	518	768	1033	1141	1339	1621	1860	2321
12500	265	483	519	769	1034	1142	1341	1623	1862	2323
15000	266	483	520	770	1034	1143	1343	1624	1863	2325
17500	266	483	521	770	1034	1143	1343	1624	1863	2325
20000	265	483	521	770	1033	1143	1343	1624	1863	2325
22500	266	484	522	770	1033	1143	1343	1625	1863	2326

TABLE 11.- LITHIUM-NUCLEUS TOTAL CROSS SECTION

Energy, MeV/amu	Lithium-nucleus total cross section, mb, for –									
	He	C	O	Al	A	Fe	Br	Ag	Ba	Pb
100	730	1263	1363	1931	2514	2769	3221	3831	4356	5358
125	695	1220	1321	1876	2445	2704	3154	3756	4276	5271
150	675	1195	1298	1845	2406	2667	3116	3714	4230	5223
175	639	1150	1255	1789	2336	2600	3047	3637	4147	5133
200	592	1092	1199	1715	2246	2512	2955	3535	4037	5014
225	564	1058	1165	1671	2192	2459	2901	3474	3971	4943
250	542	1030	1138	1635	2148	2416	2856	3424	3917	4884
275	524	1005	1114	1604	2109	2378	2817	3380	3870	4833
300	513	990	1099	1585	2086	2355	2792	3353	3840	4801
350	505	977	1087	1569	2066	2335	2772	3330	3815	4774
400	505	976	1085	1566	2063	2332	2768	3326	3811	4770
500	535	1014	1123	1615	2124	2391	2830	3396	3885	4851
600	565	1053	1161	1665	2186	2451	2893	3467	3960	4934
700	582	1075	1182	1693	2220	2484	2928	3506	4002	4980
800	595	1092	1199	1714	2247	2511	2955	3536	4035	5015
900	605	1106	1212	1732	2268	2531	2977	3560	4061	5044
1000	613	1116	1222	1745	2284	2547	2994	3579	4081	5065
1250	626	1133	1240	1767	2309	2573	3021	3609	4114	5101
1500	632	1143	1249	1778	2322	2587	3036	3626	4131	5120
1750	637	1149	1256	1786	2332	2597	3047	3637	4144	5135
2000	641	1155	1262	1794	2340	2606	3057	3648	4155	5147
2500	643	1158	1266	1798	2344	2611	3062	3654	4162	5154
3000	641	1156	1264	1795	2340	2608	3060	3650	4158	5151
3500	638	1153	1262	1791	2336	2604	3055	3646	4153	5146
4000	635	1149	1258	1787	2330	2599	3050	3640	4147	5139
5000	632	1145	1254	1781	2324	2592	3043	3633	4139	5130
6000	628	1141	1250	1776	2316	2585	3036	3625	4130	5121
7000	624	1135	1244	1769	2308	2577	3028	3615	4120	5110
8000	620	1131	1240	1763	2301	2570	3021	3607	4111	5101
9000	618	1128	1238	1760	2297	2566	3017	3603	4107	5096
10000	617	1126	1237	1758	2294	2564	3015	3600	4104	5093
12500	615	1124	1235	1755	2289	2561	3012	3597	4100	5089
15000	613	1122	1233	1752	2285	2557	3009	3593	4096	5085
17500	610	1119	1231	1748	2280	2553	3004	3588	4091	5080
20000	607	1116	1228	1744	2275	2548	3000	3583	4085	5074
22500	606	1114	1227	1742	2272	2546	2998	3581	4083	5071

TABLE 12.- LITHIUM-NUCLEUS ABSORPTION CROSS SECTION

Energy, MeV/amu	Lithium-nucleus absorption cross section, mb, for –									
	He	C	O	Al	A	Fe	Br	Ag	Ba	Pb
100	417	696	742	1047	1360	1480	1708	2026	2296	2805
125	392	665	712	1008	1311	1434	1660	1972	2238	2743
150	380	650	698	989	1287	1411	1637	1946	2210	2714
175	369	636	685	971	1265	1390	1616	1922	2184	2686
200	360	624	674	956	1247	1373	1598	1902	2163	2663
225	352	615	665	945	1232	1359	1584	1886	2146	2644
250	347	608	659	936	1222	1349	1573	1875	2133	2631
275	344	604	654	931	1215	1342	1567	1867	2125	2622
300	342	602	653	928	1212	1339	1564	1864	2121	2618
350	342	603	653	929	1212	1340	1564	1865	2123	2620
400	346	607	657	934	1219	1347	1572	1873	2131	2629
500	365	631	681	965	1258	1384	1610	1916	2177	2680
600	382	653	701	992	1292	1416	1644	1954	2217	2724
700	391	664	713	1007	1310	1434	1662	1975	2239	2748
800	398	673	721	1018	1323	1446	1675	1990	2255	2765
900	402	679	727	1026	1333	1456	1685	2001	2266	2778
1000	406	683	731	1031	1339	1462	1692	2008	2274	2786
1250	410	688	736	1037	1346	1469	1699	2016	2283	2796
1500	411	690	739	1040	1349	1473	1703	2020	2287	2800
1750	413	692	741	1042	1351	1475	1706	2023	2291	2805
2000	414	694	742	1044	1353	1477	1708	2025	2293	2807
2500	413	694	743	1043	1352	1477	1708	2025	2293	2807
3000	412	692	741	1041	1349	1475	1706	2023	2290	2804
3500	411	690	740	1039	1346	1472	1703	2019	2287	2800
4000	409	689	739	1038	1344	1470	1701	2017	2284	2798
5000	408	688	737	1036	1342	1468	1699	2015	2282	2795
6000	407	686	736	1034	1339	1466	1697	2012	2279	2792
7000	405	684	734	1031	1336	1463	1694	2009	2275	2788
8000	404	683	733	1030	1334	1461	1692	2007	2273	2786
9000	404	683	733	1029	1334	1461	1692	2007	2273	2786
10000	404	683	733	1030	1334	1461	1692	2007	2273	2786
12500	405	684	734	1031	1335	1462	1694	2009	2275	2789
15000	405	684	735	1031	1335	1463	1695	2010	2276	2790
17500	405	684	735	1031	1334	1462	1695	2009	2275	2789
20000	404	684	735	1030	1333	1462	1694	2009	2275	2789
22500	404	684	735	1031	1333	1462	1695	2009	2275	2789

TABLE 13.- BERYLLIUM-NUCLEUS TOTAL CROSS SECTION

Energy, MeV/amu	Beryllium-nucleus total cross section, mb, for –									
	He	C	O	Al	A	Fe	Br	Ag	Ba	Pb
100	804	1353	1447	2044	2656	2901	3355	3983	4518	5532
125	770	1311	1407	1991	2588	2838	3291	3911	4440	5449
150	751	1287	1385	1960	2550	2802	3255	3870	4396	5402
175	716	1243	1343	1905	2481	2737	3188	3795	4315	5315
200	670	1187	1288	1833	2392	2651	3099	3696	4209	5200
225	642	1153	1256	1790	2339	2600	3046	3637	4145	5131
250	620	1125	1229	1755	2296	2558	3003	3589	4093	5075
275	601	1101	1206	1725	2259	2522	2965	3546	4047	5025
300	589	1086	1192	1706	2235	2499	2941	3520	4019	4994
350	580	1074	1180	1690	2216	2480	2922	3498	3995	4969
400	579	1072	1178	1688	2213	2477	2919	3495	3991	4965
500	610	1110	1214	1736	2273	2535	2979	3562	4063	5044
600	640	1148	1252	1785	2334	2593	3040	3631	4136	5123
700	657	1170	1272	1812	2368	2626	3073	3669	4176	5168
800	670	1187	1289	1833	2394	2651	3100	3698	4208	5202
900	681	1200	1302	1851	2415	2672	3121	3722	4234	5230
1000	689	1211	1313	1864	2431	2688	3138	3740	4253	5252
1250	702	1228	1330	1886	2457	2714	3165	3771	4286	5287
1500	709	1238	1340	1897	2470	2728	3181	3787	4304	5307
1750	714	1244	1347	1906	2480	2738	3192	3800	4317	5321
2000	719	1251	1353	1913	2489	2747	3202	3810	4329	5334
2500	721	1254	1358	1918	2493	2753	3208	3817	4335	5342
3000	719	1252	1356	1916	2490	2750	3206	3814	4333	5339
3500	717	1250	1354	1912	2485	2746	3202	3810	4328	5334
4000	714	1246	1351	1908	2480	2741	3197	3804	4322	5327
5000	711	1242	1347	1903	2473	2735	3190	3797	4314	5319
6000	707	1238	1342	1897	2466	2728	3183	3789	4305	5310
7000	703	1232	1337	1890	2458	2720	3175	3780	4295	5299
8000	699	1228	1333	1885	2451	2714	3169	3772	4288	5291
9000	697	1226	1331	1882	2447	2710	3165	3768	4283	5287
10000	696	1224	1330	1880	2444	2708	3163	3766	4281	5284
12500	694	1222	1329	1878	2441	2705	3161	3763	4278	5281
15000	692	1221	1328	1875	2437	2703	3159	3761	4275	5279
17500	690	1218	1326	1872	2432	2699	3155	3756	4270	5274
20000	687	1215	1324	1868	2428	2695	3151	3752	4266	5269
22500	686	1214	1323	1867	2425	2693	3150	3750	4264	5267

TABLE 14.- BERYLLIUM-NUCLEUS ABSORPTION CROSS SECTION

Energy, MeV/amu	Beryllium-nucleus absorption cross section, mb, for –									
	He	C	O	Al	A	Fe	Br	Ag	Ba	Pb
100	452	739	781	1101	1430	1544	1772	2098	2373	2888
125	428	709	753	1063	1381	1498	1726	2046	2317	2828
150	416	694	739	1044	1358	1477	1704	2022	2290	2800
175	405	681	726	1027	1336	1456	1683	1998	2265	2773
200	396	669	716	1013	1318	1439	1666	1979	2244	2750
225	389	660	707	1002	1304	1426	1652	1963	2228	2733
250	384	654	701	993	1293	1416	1642	1952	2216	2720
275	381	650	697	988	1287	1410	1636	1945	2208	2711
300	379	648	695	985	1284	1407	1633	1942	2204	2708
350	379	648	696	986	1284	1408	1634	1943	2205	2709
400	383	653	700	992	1291	1414	1641	1951	2214	2718
500	402	676	723	1022	1329	1450	1678	1993	2258	2767
600	418	697	743	1048	1362	1482	1710	2029	2297	2810
700	428	709	754	1063	1381	1499	1728	2050	2319	2833
800	434	717	762	1073	1394	1512	1741	2064	2334	2850
900	439	723	768	1081	1403	1521	1751	2074	2345	2862
1000	442	728	772	1086	1410	1527	1757	2082	2353	2870
1250	446	733	777	1093	1417	1534	1765	2090	2362	2880
1500	448	735	780	1096	1420	1538	1769	2094	2367	2885
1750	450	737	782	1098	1423	1541	1772	2098	2371	2889
2000	451	739	784	1100	1424	1543	1774	2100	2373	2892
2500	451	739	785	1100	1424	1543	1775	2101	2373	2893
3000	450	738	784	1098	1421	1541	1773	2098	2371	2890
3500	448	736	782	1096	1418	1538	1770	2095	2368	2887
4000	447	735	781	1094	1416	1537	1769	2093	2365	2884
5000	446	733	780	1093	1414	1535	1767	2091	2363	2882
6000	445	732	778	1091	1411	1532	1764	2088	2360	2879
7000	443	730	776	1088	1408	1529	1761	2085	2357	2875
8000	442	729	775	1087	1406	1528	1760	2083	2354	2873
9000	442	729	775	1087	1406	1528	1759	2083	2354	2873
10000	443	729	776	1087	1406	1528	1760	2084	2355	2874
12500	443	730	777	1088	1407	1530	1762	2086	2357	2876
15000	444	731	778	1089	1408	1531	1763	2087	2358	2878
17500	443	731	779	1089	1407	1530	1764	2087	2358	2878
20000	443	731	779	1089	1406	1530	1763	2086	2358	2877
22500	443	731	779	1089	1406	1530	1764	2087	2358	2878

TABLE 15.- BORON-NUCLEUS TOTAL CROSS SECTION

Energy, MeV/amu	Boron-nucleus total cross section, mb, for –									
	He	C	O	Al	A	Fe	Br	Ag	Ba	Pb
100	856	1414	1500	2120	2755	2988	3441	4082	4622	5642
125	824	1374	1463	2068	2689	2928	3380	4012	4547	5562
150	806	1351	1441	2039	2652	2893	3345	3973	4505	5517
175	772	1309	1402	1986	2585	2830	3281	3901	4427	5434
200	727	1253	1349	1916	2498	2747	3195	3805	4325	5323
225	701	1221	1318	1874	2446	2698	3145	3748	4263	5257
250	679	1194	1293	1840	2404	2658	3103	3702	4213	5203
275	660	1170	1270	1811	2367	2622	3067	3661	4169	5156
300	648	1156	1256	1792	2344	2600	3044	3635	4142	5126
350	638	1144	1245	1777	2325	2582	3025	3615	4119	5102
400	637	1142	1243	1775	2323	2579	3022	3611	4116	5098
500	667	1179	1278	1822	2382	2635	3080	3677	4185	5174
600	697	1216	1314	1869	2441	2692	3139	3743	4256	5251
700	714	1237	1334	1896	2474	2724	3172	3780	4295	5293
800	727	1254	1350	1917	2501	2749	3198	3809	4326	5327
900	737	1267	1363	1934	2521	2769	3218	3832	4351	5354
1000	745	1278	1373	1947	2537	2784	3235	3850	4370	5375
1250	759	1295	1391	1969	2563	2810	3262	3880	4403	5410
1500	766	1305	1401	1981	2576	2825	3277	3896	4421	5430
1750	772	1312	1408	1989	2586	2835	3289	3909	4434	5445
2000	776	1318	1415	1997	2595	2844	3299	3920	4445	5458
2500	779	1322	1419	2002	2600	2850	3305	3927	4453	5466
3000	778	1321	1419	2000	2597	2848	3304	3924	4450	5464
3500	776	1318	1417	1997	2593	2844	3300	3920	4446	5459
4000	773	1315	1414	1993	2587	2840	3295	3915	4440	5453
5000	770	1311	1410	1988	2581	2833	3289	3908	4433	5445
6000	766	1306	1405	1982	2574	2827	3282	3901	4425	5436
7000	762	1301	1401	1976	2566	2819	3274	3892	4415	5426
8000	759	1297	1397	1971	2559	2813	3268	3885	4408	5418
9000	757	1295	1395	1968	2556	2810	3265	3881	4404	5414
10000	755	1294	1394	1966	2553	2808	3264	3879	4402	5412
12500	754	1293	1394	1964	2550	2806	3262	3877	4400	5410
15000	752	1291	1393	1963	2547	2804	3261	3876	4398	5409
17500	750	1289	1392	1960	2543	2801	3258	3872	4394	5405
20000	748	1287	1390	1957	2539	2798	3255	3868	4390	5400
22500	747	1286	1389	1955	2536	2796	3254	3866	4388	5399

TABLE 16.- BORON-NUCLEUS ABSORPTION CROSS SECTION

Energy, MeV/amu	Boron-nucleus absorption cross section, mb, for –									
	He	C	O	Al	A	Fe	Br	Ag	Ba	Pb
100	476	766	804	1136	1477	1584	1811	2144	2421	2939
125	453	737	777	1099	1430	1540	1766	2094	2367	2881
150	442	724	764	1081	1407	1519	1745	2070	2342	2854
175	431	710	752	1065	1386	1500	1725	2047	2317	2828
200	422	700	742	1051	1368	1483	1709	2028	2297	2806
225	415	691	734	1040	1354	1471	1696	2014	2281	2789
250	410	685	728	1032	1344	1461	1686	2003	2270	2777
275	407	681	725	1027	1337	1455	1680	1996	2262	2769
300	406	679	723	1024	1334	1452	1677	1993	2259	2765
350	406	679	724	1025	1335	1453	1678	1994	2260	2767
400	409	684	728	1031	1342	1460	1685	2002	2268	2776
500	428	707	749	1060	1379	1494	1721	2042	2311	2822
600	444	727	768	1086	1412	1525	1752	2077	2349	2863
700	453	738	779	1100	1430	1542	1770	2097	2370	2886
800	459	746	787	1110	1443	1554	1782	2111	2385	2902
900	464	752	793	1118	1452	1563	1791	2121	2396	2914
1000	468	756	797	1123	1458	1569	1798	2129	2403	2922
1250	472	762	802	1129	1465	1576	1806	2137	2412	2932
1500	474	764	805	1132	1469	1580	1810	2141	2417	2938
1750	475	767	807	1135	1472	1583	1813	2145	2421	2942
2000	477	768	809	1137	1473	1586	1816	2148	2424	2945
2500	477	769	810	1137	1473	1586	1817	2149	2424	2946
3000	476	768	809	1136	1471	1584	1815	2146	2422	2944
3500	475	766	808	1134	1468	1582	1813	2144	2419	2940
4000	474	765	807	1132	1466	1580	1811	2142	2417	2938
5000	473	764	806	1131	1464	1578	1809	2139	2415	2936
6000	471	762	804	1128	1461	1576	1806	2137	2412	2933
7000	470	760	803	1126	1459	1573	1804	2134	2409	2930
8000	469	759	802	1125	1457	1572	1802	2132	2407	2927
9000	469	759	802	1125	1456	1571	1802	2132	2407	2927
10000	469	760	803	1125	1457	1572	1803	2133	2407	2928
12500	470	761	804	1127	1458	1574	1805	2135	2410	2931
15000	471	762	806	1128	1458	1575	1807	2136	2411	2933
17500	471	762	806	1128	1458	1575	1807	2137	2411	2933
20000	471	762	806	1128	1457	1575	1807	2137	2411	2933
22500	471	762	807	1128	1458	1576	1808	2137	2412	2934

TABLE 17.- CARBON-NUCLEUS TOTAL CROSS SECTION

Energy, MeV/amu	Carbon-nucleus total cross section, mb, for –									
	He	C	O	Al	A	Fe	Br	Ag	Ba	Pb
100	880	1441	1523	2150	2802	3029	3480	4130	4671	5697
125	848	1402	1487	2099	2736	2969	3420	4062	4598	5619
150	830	1379	1466	2071	2699	2935	3386	4023	4556	5574
175	797	1338	1428	2019	2633	2873	3323	3951	4479	5491
200	753	1283	1376	1950	2546	2791	3239	3856	4378	5381
225	726	1251	1346	1909	2494	2742	3189	3800	4317	5316
250	705	1224	1321	1876	2452	2702	3148	3754	4268	5263
275	686	1201	1299	1846	2416	2667	3112	3713	4224	5215
300	674	1187	1285	1828	2393	2645	3089	3688	4197	5186
350	664	1175	1274	1813	2374	2628	3071	3667	4175	5162
400	663	1173	1272	1811	2372	2625	3068	3664	4171	5158
500	692	1209	1306	1857	2430	2680	3124	3727	4239	5231
600	722	1247	1341	1904	2489	2736	3181	3792	4309	5306
700	739	1267	1361	1930	2522	2767	3213	3828	4347	5348
800	752	1284	1377	1951	2547	2792	3239	3857	4378	5382
900	762	1297	1390	1967	2568	2812	3260	3880	4403	5408
1000	770	1307	1400	1980	2584	2827	3276	3898	4422	5429
1250	784	1325	1418	2002	2610	2853	3303	3928	4454	5465
1500	792	1335	1428	2014	2624	2868	3319	3945	4473	5485
1750	797	1342	1435	2023	2634	2878	3330	3958	4486	5500
2000	802	1348	1442	2030	2642	2887	3340	3969	4498	5513
2500	805	1352	1447	2036	2648	2894	3347	3976	4505	5522
3000	804	1351	1446	2034	2645	2892	3346	3974	4503	5520
3500	802	1349	1444	2031	2641	2888	3343	3970	4499	5516
4000	799	1346	1441	2027	2635	2884	3338	3965	4493	5509
5000	796	1341	1437	2022	2629	2877	3331	3958	4486	5501
6000	792	1337	1433	2016	2622	2871	3325	3950	4478	5493
7000	788	1332	1429	2010	2614	2863	3317	3941	4468	5483
8000	785	1328	1425	2005	2608	2857	3311	3935	4461	5475
9000	783	1326	1423	2002	2604	2854	3308	3931	4457	5471
10000	782	1325	1423	2001	2602	2853	3307	3929	4455	5469
12500	780	1324	1422	1999	2599	2851	3306	3928	4454	5467
15000	779	1323	1422	1998	2596	2849	3305	3926	4452	5466
17500	777	1321	1421	1995	2592	2846	3302	3923	4448	5462
20000	775	1319	1419	1993	2588	2843	3299	3919	4444	5458
22500	774	1318	1419	1991	2586	2842	3298	3918	4443	5457

TABLE 18.- CARBON-NUCLEUS ABSORPTION CROSS SECTION

Energy, MeV/amu	Carbon-nucleus absorption cross section, mb, for –									
	He	C	O	Al	A	Fe	Br	Ag	Ba	Pb
100	486	778	814	1148	1500	1603	1828	2166	2444	2964
125	464	750	788	1113	1453	1560	1784	2116	2391	2907
150	453	737	775	1095	1430	1539	1764	2093	2366	2880
175	442	724	763	1079	1409	1520	1744	2071	2341	2854
200	434	713	754	1066	1391	1504	1728	2052	2322	2833
225	427	705	746	1055	1377	1491	1715	2037	2306	2816
250	422	698	740	1047	1367	1481	1706	2027	2294	2804
275	419	695	737	1042	1361	1476	1700	2020	2287	2796
300	417	693	735	1040	1358	1473	1697	2017	2284	2792
350	418	693	736	1040	1358	1474	1698	2018	2285	2793
400	421	698	740	1046	1365	1480	1704	2025	2293	2802
500	439	720	761	1074	1401	1514	1739	2064	2335	2847
600	455	740	780	1099	1434	1544	1769	2099	2372	2887
700	464	751	790	1113	1452	1561	1786	2118	2392	2909
800	471	759	798	1123	1464	1573	1799	2132	2407	2925
900	475	765	803	1131	1474	1581	1808	2142	2418	2937
1000	479	769	807	1136	1480	1588	1814	2149	2426	2945
1250	483	775	813	1142	1487	1595	1822	2158	2435	2955
1500	485	777	816	1146	1491	1599	1826	2163	2440	2961
1750	487	780	819	1148	1494	1603	1830	2166	2444	2965
2000	488	781	820	1150	1495	1605	1833	2169	2447	2969
2500	488	782	821	1151	1495	1605	1834	2170	2448	2970
3000	487	781	821	1149	1493	1604	1832	2168	2445	2968
3500	486	779	819	1148	1490	1601	1830	2165	2443	2965
4000	485	778	818	1146	1488	1599	1828	2163	2440	2963
5000	484	777	817	1144	1486	1598	1826	2161	2438	2960
6000	483	775	816	1143	1484	1595	1824	2159	2435	2957
7000	482	774	814	1140	1481	1593	1821	2156	2432	2954
8000	481	773	813	1139	1479	1591	1820	2154	2430	2952
9000	481	773	814	1139	1479	1591	1820	2154	2430	2952
10000	481	773	814	1140	1479	1592	1821	2154	2431	2953
12500	482	775	816	1141	1480	1594	1823	2157	2433	2955
15000	483	776	818	1142	1481	1595	1825	2159	2435	2958
17500	483	776	818	1143	1481	1595	1825	2159	2435	2958
20000	483	776	818	1143	1480	1595	1826	2159	2435	2958
22500	483	777	819	1143	1481	1596	1826	2160	2436	2959

TABLE 19.- NITROGEN-NUCLEUS TOTAL CROSS SECTION

Energy, MeV/amu	Nitrogen-nucleus total cross section, mb, for –									
	He	C	O	Al	A	Fe	Br	Ag	Ba	Pb
100	914	1480	1554	2195	2870	3084	3526	4190	4736	5762
125	884	1442	1520	2147	2805	3027	3470	4125	4665	5687
150	867	1421	1501	2120	2769	2994	3437	4087	4625	5644
175	835	1381	1464	2069	2704	2934	3377	4018	4551	5565
200	793	1328	1415	2003	2620	2855	3297	3927	4453	5460
225	767	1297	1386	1964	2569	2808	3249	3873	4395	5397
250	746	1271	1362	1932	2528	2769	3210	3829	4348	5346
275	728	1249	1341	1903	2493	2736	3175	3789	4306	5300
300	716	1235	1328	1886	2470	2715	3154	3765	4280	5272
350	707	1223	1317	1871	2452	2697	3136	3745	4258	5249
400	705	1222	1315	1869	2450	2695	3133	3742	4255	5246
500	734	1257	1348	1914	2507	2748	3187	3804	4321	5317
600	763	1293	1382	1959	2564	2802	3242	3866	4388	5389
700	779	1313	1401	1984	2597	2833	3273	3901	4425	5430
800	792	1329	1416	2004	2622	2857	3298	3929	4455	5462
900	802	1342	1429	2021	2643	2876	3318	3952	4480	5488
1000	810	1352	1438	2033	2658	2891	3334	3969	4498	5508
1250	824	1370	1456	2055	2684	2917	3361	3999	4530	5544
1500	831	1380	1466	2067	2698	2932	3376	4016	4549	5564
1750	837	1387	1474	2076	2708	2943	3388	4029	4562	5579
2000	842	1394	1481	2084	2717	2952	3398	4040	4574	5592
2500	845	1398	1486	2089	2722	2958	3406	4048	4582	5601
3000	845	1397	1486	2088	2720	2957	3405	4046	4580	5600
3500	843	1395	1484	2086	2716	2954	3402	4043	4577	5596
4000	840	1392	1481	2082	2711	2949	3397	4038	4571	5590
5000	837	1388	1478	2077	2705	2943	3391	4031	4564	5582
6000	834	1384	1474	2071	2698	2937	3385	4024	4556	5574
7000	830	1379	1469	2065	2690	2930	3378	4015	4547	5564
8000	827	1375	1466	2061	2684	2924	3372	4009	4540	5557
9000	825	1374	1464	2058	2680	2921	3370	4006	4537	5553
10000	824	1373	1464	2057	2678	2920	3368	4004	4535	5552
12500	823	1372	1464	2056	2676	2919	3368	4003	4534	5551
15000	822	1371	1465	2055	2674	2918	3368	4003	4533	5551
17500	820	1370	1464	2053	2670	2915	3366	4000	4530	5548
20000	819	1368	1463	2051	2666	2913	3363	3997	4527	5545
22500	818	1367	1462	2050	2664	2911	3363	3996	4526	5543

TABLE 20.- NITROGEN-NUCLEUS ABSORPTION CROSS SECTION

Energy, MeV/amu	Nitrogen-nucleus absorption cross section, mb, for –									
	He	C	O	Al	A	Fe	Br	Ag	Ba	Pb
100	501	795	824	1167	1531	1627	1845	2192	2472	2992
125	479	768	800	1133	1485	1586	1804	2145	2421	2937
150	469	755	789	1116	1463	1566	1785	2122	2397	2911
175	459	742	778	1101	1443	1547	1766	2100	2374	2887
200	451	732	769	1088	1425	1531	1751	2083	2355	2866
225	444	724	761	1078	1412	1519	1739	2069	2340	2850
250	440	718	756	1070	1402	1510	1730	2058	2329	2838
275	437	715	753	1066	1396	1505	1724	2052	2321	2831
300	435	713	751	1063	1393	1502	1722	2049	2318	2828
350	436	714	752	1064	1393	1503	1723	2050	2319	2829
400	439	718	756	1069	1400	1509	1729	2057	2327	2837
500	457	739	776	1097	1436	1542	1762	2095	2368	2881
600	472	759	794	1121	1467	1571	1791	2128	2404	2919
700	481	769	804	1135	1485	1588	1808	2147	2424	2941
800	487	777	811	1144	1497	1599	1819	2160	2438	2956
900	491	783	816	1151	1506	1608	1828	2170	2449	2967
1000	495	787	820	1157	1513	1614	1834	2177	2456	2975
1250	499	792	826	1163	1520	1621	1842	2186	2465	2986
1500	501	795	829	1166	1524	1625	1847	2191	2470	2992
1750	503	798	832	1169	1527	1629	1851	2195	2475	2996
2000	504	799	834	1171	1529	1631	1854	2198	2478	3000
2500	505	800	835	1172	1529	1632	1855	2199	2479	3001
3000	504	799	834	1171	1527	1631	1854	2197	2477	2999
3500	503	798	833	1169	1524	1629	1852	2195	2474	2997
4000	502	797	832	1168	1522	1627	1850	2193	2472	2995
5000	501	796	831	1166	1520	1625	1848	2191	2470	2992
6000	500	794	830	1164	1518	1623	1846	2188	2467	2989
7000	499	793	829	1163	1515	1620	1844	2186	2464	2986
8000	498	792	828	1161	1513	1619	1842	2184	2463	2984
9000	498	792	828	1161	1513	1619	1843	2184	2463	2984
10000	498	792	829	1162	1514	1620	1844	2185	2464	2985
12500	500	794	831	1164	1515	1622	1846	2188	2466	2989
15000	501	795	833	1165	1516	1623	1848	2189	2468	2991
17500	501	796	834	1166	1516	1624	1849	2190	2469	2992
20000	501	796	834	1166	1515	1624	1849	2190	2469	2992
22500	501	797	835	1166	1516	1625	1850	2191	2470	2993

TABLE 21.- OXYGEN-NUCLEUS TOTAL CROSS SECTION

Energy, MeV/amu	Oxygen-nucleus total cross section, mb, for –									
	He	C	O	Al	À	Fe	Br	Ag	Ba	Pb
100	954	1526	1594	2252	2946	3153	3591	4268	4819	5849
125	924	1490	1562	2205	2883	3096	3537	4204	4750	5776
150	907	1469	1544	2179	2847	3065	3505	4167	4710	5734
175	876	1430	1509	2130	2783	3006	3447	4100	4638	5657
200	834	1379	1461	2065	2699	2928	3369	4010	4542	5554
225	809	1348	1433	2026	2649	2882	3322	3957	4485	5493
250	789	1323	1409	1994	2609	2844	3284	3914	4439	5443
275	771	1301	1389	1967	2574	2811	3250	3876	4398	5399
300	759	1287	1376	1949	2552	2791	3229	3852	4373	5372
350	750	1276	1365	1935	2534	2774	3212	3833	4352	5349
400	748	1274	1364	1933	2531	2771	3209	3830	4349	5346
500	776	1309	1396	1977	2588	2824	3262	3890	4413	5415
600	804	1344	1428	2021	2645	2877	3316	3951	4479	5486
700	821	1364	1447	2046	2677	2907	3346	3986	4516	5526
800	833	1380	1462	2066	2703	2931	3371	4014	4546	5558
900	844	1393	1474	2082	2723	2950	3390	4036	4570	5584
1000	852	1403	1484	2095	2738	2965	3406	4053	4588	5604
1250	866	1420	1501	2116	2764	2991	3433	4083	4620	5639
1500	874	1430	1512	2129	2779	3006	3449	4100	4639	5659
1750	880	1438	1520	2138	2789	3017	3461	4114	4652	5675
2000	885	1444	1527	2146	2798	3026	3471	4125	4664	5688
2500	888	1449	1532	2152	2803	3033	3479	4133	4673	5697
3000	888	1449	1533	2151	2801	3032	3478	4131	4671	5696
3500	886	1447	1531	2148	2797	3029	3475	4128	4668	5693
4000	884	1444	1529	2145	2793	3024	3471	4123	4662	5687
5000	880	1440	1525	2140	2786	3019	3465	4116	4655	5679
6000	877	1436	1521	2135	2780	3012	3459	4109	4648	5671
7000	873	1431	1517	2129	2772	3005	3452	4101	4639	5662
8000	870	1427	1514	2124	2766	3000	3447	4095	4632	5655
9000	868	1426	1512	2122	2762	2997	3444	4092	4629	5652
10000	868	1425	1512	2121	2760	2996	3443	4091	4628	5650
12500	867	1425	1513	2120	2758	2995	3443	4090	4627	5650
15000	866	1424	1514	2120	2756	2995	3444	4090	4627	5650
17500	865	1423	1513	2118	2753	2993	3442	4088	4624	5648
20000	863	1421	1512	2116	2749	2990	3440	4085	4621	5645
22500	863	1421	1512	2115	2748	2989	3440	4084	4620	5644

TABLE 22.- OXYGEN-NUCLEUS ABSORPTION CROSS SECTION

Energy, MeV/amu	Oxygen-nucleus absorption cross section, mb, for –									
	He	C	O	Al	A	Fe	Br	Ag	Ba	Pb
100	519	816	842	1194	1569	1659	1875	2229	2511	3032
125	498	790	819	1160	1523	1619	1835	2182	2461	2979
150	488	777	808	1144	1501	1599	1816	2160	2438	2954
175	478	765	797	1129	1481	1581	1799	2139	2415	2930
200	470	755	789	1117	1464	1566	1784	2122	2396	2910
225	464	748	782	1107	1451	1554	1772	2108	2382	2895
250	459	742	777	1099	1441	1545	1763	2098	2371	2883
275	456	738	774	1095	1435	1540	1758	2092	2364	2876
300	455	737	772	1093	1432	1537	1756	2089	2361	2873
350	456	737	773	1093	1433	1538	1756	2090	2362	2874
400	459	741	777	1099	1439	1544	1763	2097	2370	2882
500	476	763	796	1126	1475	1577	1795	2134	2410	2925
600	491	782	813	1149	1506	1605	1823	2167	2445	2962
700	500	792	823	1163	1523	1621	1839	2185	2464	2983
800	506	800	830	1172	1536	1633	1851	2198	2479	2999
900	510	805	835	1179	1545	1641	1859	2208	2489	3010
1000	514	809	839	1184	1551	1647	1866	2215	2496	3018
1250	518	815	845	1191	1559	1655	1874	2224	2506	3028
1500	520	818	848	1194	1562	1659	1878	2229	2511	3034
1750	522	821	851	1197	1566	1663	1882	2233	2516	3039
2000	524	822	853	1199	1568	1665	1885	2236	2519	3043
2500	524	823	855	1201	1568	1666	1887	2238	2520	3044
3000	524	823	854	1199	1566	1665	1886	2236	2518	3043
3500	523	821	853	1198	1563	1663	1884	2234	2516	3040
4000	522	820	852	1196	1561	1661	1882	2232	2514	3038
5000	521	819	851	1195	1559	1659	1881	2230	2512	3036
6000	520	818	850	1193	1557	1657	1879	2227	2509	3033
7000	519	816	849	1191	1554	1655	1876	2225	2506	3030
8000	518	815	848	1190	1553	1654	1875	2223	2504	3028
9000	518	815	849	1190	1552	1654	1875	2223	2504	3028
10000	518	816	849	1191	1553	1654	1876	2224	2506	3029
12500	520	818	852	1193	1554	1657	1879	2227	2508	3033
15000	521	819	854	1194	1555	1659	1881	2229	2511	3035
17500	521	820	854	1195	1555	1659	1882	2230	2511	3036
20000	521	820	855	1195	1555	1659	1883	2230	2512	3037
22500	522	821	856	1196	1556	1660	1884	2231	2513	3038

TABLE 23.- NEON-NUCLEUS TOTAL CROSS SECTION

Energy, MeV/amu	Neon-nucleus total cross section, mb, for –									
	He	C	O	Al	A	Fe	Br	Ag	Ba	Pb
100	1076	1682	1751	2454	3174	3381	3842	4534	5102	6160
125	1045	1644	1718	2406	3109	3324	3785	4468	5032	6086
150	1028	1623	1699	2378	3072	3291	3753	4431	4992	6043
175	994	1582	1662	2326	3005	3231	3693	4362	4918	5965
200	950	1529	1613	2259	2919	3151	3612	4271	4821	5861
225	924	1496	1583	2218	2868	3104	3565	4217	4763	5799
250	902	1470	1559	2186	2826	3065	3525	4173	4716	5748
275	882	1447	1538	2157	2790	3031	3491	4134	4674	5704
300	870	1433	1524	2139	2768	3010	3469	4110	4648	5676
350	860	1421	1513	2124	2749	2993	3452	4090	4627	5653
400	858	1419	1511	2122	2747	2991	3449	4088	4624	5650
500	888	1455	1545	2168	2805	3045	3504	4149	4690	5721
600	918	1492	1579	2214	2864	3099	3559	4212	4757	5793
700	935	1513	1598	2240	2897	3130	3591	4247	4795	5833
800	949	1530	1614	2261	2923	3155	3616	4275	4825	5866
900	960	1543	1627	2278	2944	3175	3636	4298	4850	5892
1000	968	1554	1637	2291	2960	3190	3652	4316	4869	5913
1250	983	1572	1655	2314	2987	3216	3680	4347	4901	5948
1500	992	1583	1666	2327	3002	3232	3696	4365	4920	5969
1750	998	1591	1675	2336	3013	3243	3709	4378	4935	5985
2000	1003	1598	1682	2345	3022	3253	3719	4389	4946	5998
2500	1007	1603	1688	2351	3028	3260	3727	4398	4955	6008
3000	1007	1602	1688	2350	3025	3259	3727	4397	4954	6007
3500	1005	1600	1686	2347	3022	3256	3724	4393	4950	6003
4000	1002	1597	1684	2343	3017	3251	3719	4388	4945	5998
5000	999	1593	1680	2338	3010	3245	3713	4381	4938	5990
6000	995	1589	1676	2333	3003	3239	3707	4374	4930	5982
7000	991	1584	1672	2326	2995	3232	3700	4366	4921	5972
8000	988	1580	1668	2322	2989	3226	3694	4360	4915	5965
9000	986	1579	1667	2319	2986	3224	3692	4357	4911	5962
10000	986	1578	1667	2318	2984	3223	3691	4355	4910	5961
12500	985	1578	1668	2318	2982	3222	3691	4355	4910	5961
15000	984	1578	1669	2317	2980	3222	3692	4355	4909	5961
17500	983	1576	1668	2315	2976	3220	3690	4353	4907	5959
20000	981	1575	1667	2313	2973	3217	3688	4350	4904	5956
22500	980	1574	1667	2313	2971	3216	3688	4350	4903	5956

TABLE 24.- NEON-NUCLEUS ABSORPTION CROSS SECTION

Energy, MeV/amu	Neon-nucleus absorption cross section, mb, for –									
	He	C	O	Al	A	Fe	Br	Ag	Ba	Pb
100	582	896	922	1300	1686	1776	2005	2364	2655	3190
125	560	869	898	1264	1639	1734	1963	2316	2605	3136
150	549	856	887	1247	1616	1715	1944	2294	2580	3110
175	539	843	876	1231	1595	1696	1925	2272	2557	3086
200	531	833	867	1218	1578	1680	1910	2255	2538	3066
225	524	825	860	1208	1564	1668	1898	2241	2523	3050
250	519	819	854	1200	1554	1659	1889	2231	2512	3038
275	516	815	851	1195	1547	1653	1883	2224	2505	3031
300	515	814	850	1193	1544	1651	1880	2221	2502	3028
350	515	814	850	1194	1545	1652	1881	2222	2503	3029
400	519	819	854	1199	1552	1658	1888	2230	2511	3037
500	537	841	874	1228	1589	1691	1921	2268	2552	3081
600	553	860	892	1253	1621	1721	1951	2301	2588	3119
700	562	871	902	1267	1639	1737	1967	2320	2608	3140
800	568	879	910	1277	1652	1749	1979	2333	2622	3156
900	573	885	915	1284	1661	1758	1988	2343	2633	3167
1000	577	889	919	1289	1668	1764	1995	2350	2641	3176
1250	581	895	925	1296	1675	1772	2003	2360	2650	3186
1500	584	898	928	1300	1679	1776	2008	2365	2656	3192
1750	586	901	931	1303	1683	1780	2012	2369	2660	3197
2000	587	903	934	1305	1685	1783	2015	2372	2663	3201
2500	588	904	935	1306	1685	1784	2017	2374	2665	3203
3000	588	903	935	1305	1683	1782	2015	2372	2663	3201
3500	586	902	934	1303	1680	1780	2014	2370	2661	3199
4000	586	901	933	1302	1678	1779	2012	2368	2659	3196
5000	585	900	932	1300	1676	1777	2010	2366	2656	3194
6000	583	898	931	1298	1674	1774	2008	2363	2654	3191
7000	582	897	929	1296	1671	1772	2006	2361	2651	3188
8000	581	896	929	1295	1669	1771	2004	2359	2649	3186
9000	581	896	929	1295	1669	1771	2004	2359	2649	3187
10000	582	897	930	1296	1669	1772	2006	2360	2650	3188
12500	583	899	932	1298	1671	1774	2009	2363	2653	3191
15000	585	900	934	1300	1672	1776	2011	2365	2656	3194
17500	585	901	935	1300	1672	1776	2012	2366	2656	3195
20000	585	901	936	1301	1672	1777	2012	2366	2657	3196
22500	586	902	937	1301	1673	1778	2014	2368	2658	3197

TABLE 25.- ALUMINUM-NUCLEUS TOTAL CROSS SECTION

Energy, MeV/amu	Aluminum-nucleus total cross section, mb, for –									
	He	C	O	Al	A	Fe	Br	Ag	Ba	Pb
100	1432	2150	2252	3021	3798	4055	4578	5324	5942	7095
125	1389	2099	2205	2959	3721	3984	4507	5244	5857	7005
150	1365	2071	2179	2924	3677	3944	4467	5199	5809	6954
175	1321	2019	2130	2861	3599	3871	4392	5117	5721	6860
200	1262	1950	2065	2778	3497	3775	4295	5009	5606	6738
225	1226	1909	2026	2728	3437	3718	4237	4944	5537	6665
250	1197	1876	1994	2688	3388	3671	4189	4892	5482	6605
275	1171	1846	1967	2653	3345	3631	4148	4846	5433	6553
300	1155	1828	1949	2631	3319	3605	4122	4817	5402	6520
350	1141	1813	1935	2613	3297	3585	4101	4794	5378	6494
400	1139	1811	1933	2610	3294	3582	4098	4791	5374	6490
500	1178	1857	1977	2666	3363	3647	4164	4864	5452	6574
600	1218	1904	2021	2723	3432	3712	4231	4938	5530	6658
700	1240	1930	2046	2755	3470	3749	4269	4980	5575	6706
800	1258	1951	2066	2780	3501	3778	4298	5013	5610	6743
900	1272	1967	2082	2800	3525	3801	4322	5039	5638	6773
1000	1283	1980	2095	2815	3543	3819	4341	5060	5659	6797
1250	1301	2002	2116	2841	3574	3849	4372	5094	5696	6836
1500	1311	2014	2129	2856	3590	3866	4390	5113	5716	6858
1750	1318	2023	2138	2866	3602	3878	4404	5128	5731	6875
2000	1325	2030	2146	2875	3612	3889	4415	5140	5744	6889
2500	1328	2036	2152	2881	3618	3896	4423	5148	5753	6899
3000	1327	2034	2151	2879	3614	3894	4421	5146	5750	6896
3500	1324	2031	2148	2876	3610	3890	4417	5141	5746	6891
4000	1321	2027	2145	2871	3604	3884	4411	5135	5739	6884
5000	1316	2022	2140	2865	3596	3877	4404	5127	5730	6875
6000	1311	2016	2135	2858	3588	3869	4396	5119	5722	6866
7000	1306	2010	2129	2850	3579	3860	4387	5109	5711	6855
8000	1301	2005	2124	2845	3571	3854	4381	5101	5703	6846
9000	1299	2002	2122	2841	3567	3850	4377	5097	5698	6842
10000	1297	2001	2121	2839	3564	3848	4375	5095	5696	6839
12500	1295	1999	2120	2838	3561	3846	4374	5093	5694	6838
15000	1293	1998	2120	2836	3558	3844	4373	5091	5693	6836
17500	1290	1995	2118	2832	3553	3841	4370	5088	5688	6832
20000	1287	1993	2116	2829	3548	3837	4366	5084	5684	6828
22500	1286	1991	2115	2828	3546	3835	4365	5082	5682	6826

TABLE 26.- ALUMINUM-NUCLEUS ABSORPTION CROSS SECTION

Energy, MeV/amu	Aluminum-nucleus absorption cross section, mb, for –									
	He	C	O	Al	A	Fe	Br	Ag	Ba	Pb
100	778	1148	1194	1601	2015	2132	2394	2780	3096	3680
125	747	1113	1160	1557	1960	2081	2343	2723	3035	3615
150	733	1095	1144	1536	1933	2057	2318	2695	3006	3585
175	719	1079	1129	1516	1908	2034	2295	2670	2979	3555
200	707	1066	1117	1500	1888	2015	2276	2648	2956	3531
225	698	1055	1107	1487	1872	2000	2261	2631	2938	3512
250	691	1047	1099	1477	1859	1989	2250	2619	2925	3498
275	687	1042	1095	1471	1852	1982	2243	2611	2916	3489
300	685	1040	1093	1468	1848	1979	2240	2608	2913	3485
350	686	1040	1093	1469	1849	1980	2241	2609	2914	3487
400	690	1046	1099	1476	1857	1988	2249	2617	2923	3497
500	714	1074	1126	1511	1900	2028	2289	2663	2971	3548
600	736	1099	1149	1541	1938	2063	2325	2703	3014	3594
700	748	1113	1163	1558	1959	2083	2345	2725	3037	3619
800	756	1123	1172	1570	1974	2097	2360	2741	3054	3637
900	762	1131	1179	1579	1985	2107	2370	2753	3066	3650
1000	766	1136	1184	1586	1992	2114	2378	2761	3075	3660
1250	772	1142	1191	1593	2001	2123	2387	2771	3085	3671
1500	774	1146	1194	1597	2005	2128	2392	2776	3091	3677
1750	777	1148	1197	1600	2008	2131	2396	2780	3095	3682
2000	778	1150	1199	1602	2010	2134	2399	2783	3099	3685
2500	778	1151	1201	1603	2010	2134	2400	2784	3099	3686
3000	777	1149	1199	1601	2007	2132	2398	2781	3097	3684
3500	775	1148	1198	1599	2004	2129	2395	2778	3094	3680
4000	774	1146	1196	1597	2001	2127	2393	2776	3091	3678
5000	773	1144	1195	1595	1999	2125	2391	2774	3088	3675
6000	771	1143	1193	1592	1996	2122	2388	2770	3085	3672
7000	769	1140	1191	1590	1993	2119	2385	2767	3082	3668
8000	768	1139	1190	1588	1991	2118	2383	2765	3079	3666
9000	768	1139	1190	1588	1990	2117	2383	2765	3079	3666
10000	768	1140	1191	1589	1991	2118	2384	2766	3080	3667
12500	769	1141	1193	1590	1992	2120	2387	2769	3083	3670
15000	770	1142	1194	1592	1993	2122	2389	2770	3085	3672
17500	770	1143	1195	1592	1992	2122	2389	2770	3085	3672
20000	770	1143	1195	1591	1992	2122	2389	2770	3085	3672
22500	770	1143	1196	1592	1992	2122	2390	2771	3085	3673

TABLE 27.- ARGON-NUCLEUS TOTAL CROSS SECTION

Energy, MeV/amu	Argon-nucleus total cross section, mb, for –									
	He	C	O	Al	A	Fe	Br	Ag	Ba	Pb
100	1927	2780	2915	3773	4628	4934	5524	6338	7016	8275
125	1871	2717	2854	3698	4537	4849	5439	6244	6916	8170
150	1840	2681	2820	3655	4486	4801	5390	6191	6860	8111
175	1782	2615	2758	3579	4395	4714	5302	6095	6758	8003
200	1706	2530	2676	3479	4277	4601	5187	5969	6625	7862
225	1661	2479	2627	3419	4207	4534	5118	5894	6545	7777
250	1624	2438	2588	3371	4150	4479	5062	5833	6481	7709
275	1591	2402	2553	3329	4100	4432	5014	5780	6424	7649
300	1570	2379	2531	3302	4070	4402	4984	5747	6390	7612
350	1553	2361	2514	3281	4045	4378	4959	5720	6361	7582
400	1549	2358	2511	3278	4041	4375	4955	5717	6357	7578
500	1599	2415	2566	3345	4121	4451	5034	5803	6447	7676
600	1650	2472	2621	3413	4202	4528	5113	5890	6538	7774
700	1678	2504	2653	3451	4246	4571	5157	5938	6589	7828
800	1701	2530	2677	3480	4281	4605	5192	5976	6629	7871
900	1719	2550	2697	3504	4309	4632	5220	6006	6661	7905
1000	1732	2565	2712	3522	4330	4652	5241	6029	6686	7931
1250	1754	2591	2738	3552	4364	4687	5277	6068	6726	7974
1500	1766	2605	2752	3569	4382	4705	5296	6088	6749	7998
1750	1774	2615	2762	3580	4395	4719	5310	6104	6765	8016
2000	1782	2624	2771	3590	4406	4730	5323	6117	6779	8031
2500	1786	2629	2777	3596	4413	4737	5331	6125	6788	8041
3000	1783	2627	2775	3594	4408	4734	5328	6122	6784	8037
3500	1779	2623	2772	3589	4403	4729	5323	6116	6778	8031
4000	1775	2618	2767	3583	4396	4722	5316	6109	6770	8023
5000	1769	2611	2761	3576	4387	4714	5308	6100	6760	8013
6000	1763	2605	2754	3568	4378	4705	5299	6090	6750	8002
7000	1756	2597	2747	3558	4366	4695	5288	6078	6738	7989
8000	1750	2590	2741	3551	4358	4687	5280	6069	6728	7979
9000	1746	2587	2738	3547	4353	4682	5275	6064	6723	7973
10000	1744	2585	2736	3545	4349	4679	5273	6062	6720	7970
12500	1741	2582	2734	3541	4345	4676	5270	6058	6717	7967
15000	1737	2579	2732	3539	4340	4673	5268	6055	6713	7964
17500	1733	2575	2729	3534	4334	4668	5263	6050	6708	7958
20000	1729	2571	2726	3529	4329	4663	5258	6045	6702	7953
22500	1726	2569	2724	3527	4325	4661	5256	6042	6699	7950

TABLE 28.-ARGON-NUCLEUS ABSORPTION CROSS SECTION

Energy, MeV/amu	Argon-nucleus absorption cross section, mb, for –									
	He	C	O	Al	A	Fe	Br	Ag	Ba	Pb
100	1044	1483	1546	1997	2449	2592	2888	3308	3654	4293
125	1005	1438	1503	1944	2384	2532	2827	3241	3583	4217
150	986	1416	1482	1918	2354	2503	2798	3209	3550	4182
175	967	1396	1463	1894	2325	2475	2770	3179	3518	4148
200	952	1379	1446	1874	2301	2453	2748	3154	3491	4120
225	941	1366	1434	1858	2282	2435	2730	3134	3470	4098
250	932	1356	1424	1846	2268	2422	2716	3119	3455	4082
275	926	1349	1418	1839	2259	2414	2708	3110	3445	4072
300	924	1346	1416	1836	2255	2410	2704	3106	3440	4067
350	924	1347	1416	1837	2256	2411	2705	3108	3442	4069
400	930	1354	1423	1844	2265	2420	2715	3118	3452	4080
500	961	1389	1457	1886	2315	2467	2763	3171	3508	4140
600	988	1420	1487	1923	2359	2509	2806	3218	3558	4193
700	1003	1438	1503	1943	2384	2532	2830	3244	3585	4223
800	1014	1450	1515	1958	2401	2549	2846	3262	3604	4243
900	1022	1459	1524	1968	2413	2560	2859	3276	3618	4258
1000	1027	1465	1530	1976	2422	2569	2867	3285	3628	4269
1250	1033	1472	1537	1984	2431	2578	2877	3296	3639	4281
1500	1036	1476	1541	1988	2435	2583	2882	3301	3645	4287
1750	1038	1479	1544	1991	2439	2587	2886	3305	3650	4292
2000	1040	1481	1546	1994	2441	2589	2889	3308	3653	4295
2500	1040	1481	1547	1994	2440	2590	2890	3308	3653	4296
3000	1038	1478	1545	1991	2437	2586	2887	3305	3649	4292
3500	1035	1476	1543	1988	2433	2583	2883	3301	3646	4288
4000	1034	1474	1541	1986	2430	2581	2881	3299	3643	4285
5000	1032	1472	1539	1983	2427	2578	2878	3296	3640	4282
6000	1030	1469	1537	1981	2424	2575	2875	3292	3636	4278
7000	1027	1467	1534	1977	2420	2571	2871	3288	3632	4274
8000	1026	1465	1533	1975	2418	2569	2869	3286	3629	4271
9000	1025	1465	1533	1975	2417	2568	2869	3285	3629	4270
10000	1026	1465	1533	1975	2417	2569	2870	3286	3629	4271
12500	1027	1467	1535	1977	2419	2571	2872	3289	3632	4274
15000	1027	1468	1536	1978	2419	2572	2873	3290	3633	4276
17500	1026	1467	1536	1978	2418	2572	2873	3290	3633	4276
20000	1026	1467	1536	1977	2417	2571	2873	3289	3632	4275
22500	1026	1467	1537	1978	2417	2572	2874	3290	3633	4276

TABLE 29.- IRON-NUCLEUS TOTAL CROSS SECTION

Energy, MeV/amu	Iron-nucleus total cross section, mb, for –									
	He	C	O	Al	A	Fe	Br	Ag	Ba	Pb
100	2149	3022	3139	4054	4967	5247	5836	6682	7377	8654
125	2097	2963	3084	3983	4879	5167	5757	6594	7283	8556
150	2068	2929	3052	3943	4830	5122	5711	6544	7230	8500
175	2013	2868	2994	3870	4741	5039	5628	6453	7133	8399
200	1940	2786	2918	3774	4626	4931	5520	6333	7007	8265
225	1896	2738	2872	3717	4558	4867	5455	6262	6932	8186
250	1860	2698	2835	3671	4503	4815	5402	6204	6871	8122
275	1828	2663	2802	3630	4454	4769	5356	6154	6817	8065
300	1808	2641	2781	3605	4424	4741	5328	6123	6784	8030
350	1790	2624	2765	3584	4400	4718	5304	6097	6757	8002
400	1787	2621	2762	3581	4397	4715	5301	6094	6754	7998
500	1835	2675	2814	3646	4475	4788	5375	6176	6840	8090
600	1884	2731	2866	3711	4553	4862	5450	6258	6927	8183
700	1912	2762	2896	3748	4597	4903	5493	6305	6975	8235
800	1934	2786	2920	3777	4632	4936	5526	6341	7014	8276
900	1951	2806	2939	3800	4659	4962	5553	6371	7045	8309
1000	1965	2821	2953	3818	4680	4983	5574	6393	7069	8334
1250	1988	2847	2979	3848	4715	5017	5609	6431	7109	8377
1500	2000	2862	2994	3865	4733	5036	5629	6453	7132	8402
1750	2009	2873	3005	3877	4747	5050	5644	6469	7149	8420
2000	2017	2882	3014	3888	4758	5062	5657	6482	7163	8436
2500	2022	2888	3021	3895	4765	5070	5666	6492	7173	8446
3000	2020	2886	3020	3893	4762	5068	5664	6489	7170	8444
3500	2017	2883	3017	3889	4756	5063	5660	6484	7165	8439
4000	2012	2878	3013	3883	4750	5057	5653	6478	7158	8431
5000	2007	2872	3007	3876	4741	5049	5645	6469	7148	8421
6000	2001	2865	3001	3869	4732	5041	5637	6460	7139	8411
7000	1994	2858	2994	3860	4721	5031	5627	6448	7127	8399
8000	1989	2852	2989	3853	4713	5023	5620	6440	7118	8390
9000	1986	2849	2986	3849	4708	5019	5616	6436	7114	8385
10000	1984	2847	2985	3847	4705	5017	5614	6434	7111	8383
12500	1981	2846	2985	3845	4702	5015	5613	6432	7110	8382
15000	1979	2844	2984	3844	4699	5014	5612	6431	7108	8380
17500	1975	2841	2982	3840	4693	5010	5608	6427	7104	8376
20000	1972	2838	2980	3836	4688	5006	5605	6423	7099	8372
22500	1970	2837	2979	3835	4686	5004	5604	6421	7098	8370

TABLE 30.- IRON-NUCLEUS ABSORPTION CROSS SECTION

Energy, MeV/amu	Iron-nucleus absorption cross section, mb, for –									
	He	C	O	Al	A	Fe	Br	Ag	Ba	Pb
100	1149	1598	1649	2131	2615	2742	3036	3472	3827	4473
125	1112	1555	1610	2081	2552	2685	2979	3409	3760	4402
150	1094	1535	1591	2056	2522	2657	2951	3379	3728	4369
175	1077	1516	1573	2034	2494	2631	2925	3350	3698	4337
200	1063	1500	1558	2015	2471	2610	2904	3326	3673	4311
225	1052	1487	1546	2000	2452	2593	2887	3308	3653	4290
250	1043	1478	1538	1989	2439	2581	2875	3294	3638	4275
275	1038	1472	1532	1982	2430	2573	2867	3285	3629	4265
300	1036	1469	1530	1979	2426	2569	2864	3282	3625	4261
350	1037	1470	1531	1979	2427	2570	2865	3283	3626	4263
400	1042	1476	1537	1987	2436	2579	2874	3293	3637	4274
500	1072	1510	1569	2027	2485	2624	2920	3344	3690	4330
600	1098	1540	1597	2062	2528	2664	2960	3388	3737	4380
700	1112	1556	1612	2082	2552	2687	2983	3413	3763	4408
800	1123	1568	1624	2096	2569	2702	2999	3431	3782	4428
900	1130	1577	1632	2106	2581	2714	3010	3444	3795	4443
1000	1136	1583	1638	2113	2590	2722	3019	3453	3805	4453
1250	1142	1590	1645	2122	2599	2732	3029	3464	3816	4465
1500	1145	1594	1650	2127	2604	2737	3035	3469	3823	4472
1750	1148	1598	1653	2130	2608	2741	3039	3474	3828	4477
2000	1150	1600	1656	2133	2610	2744	3042	3478	3831	4481
2500	1150	1601	1657	2134	2610	2745	3044	3479	3832	4483
3000	1148	1599	1656	2131	2607	2742	3041	3476	3829	4480
3500	1146	1597	1654	2129	2603	2740	3038	3472	3826	4476
4000	1145	1595	1652	2126	2601	2737	3036	3470	3823	4473
5000	1143	1593	1650	2124	2598	2735	3034	3467	3820	4470
6000	1141	1591	1648	2122	2595	2732	3030	3464	3816	4466
7000	1139	1588	1646	2119	2591	2728	3027	3460	3813	4462
8000	1137	1587	1645	2117	2589	2726	3025	3458	3810	4460
9000	1137	1587	1645	2117	2588	2726	3025	3458	3810	4460
10000	1138	1587	1646	2117	2589	2727	3026	3459	3811	4461
12500	1139	1589	1648	2119	2590	2729	3029	3462	3814	4465
15000	1140	1591	1650	2121	2591	2731	3031	3464	3816	4467
17500	1140	1591	1651	2121	2591	2731	3032	3464	3816	4468
20000	1140	1591	1651	2121	2590	2731	3032	3464	3816	4468
22500	1140	1592	1652	2122	2590	2732	3033	3465	3818	4469

TABLE 31.- COPPER-NUCLEUS TOTAL CROSS SECTION

Energy, MeV/amu	Copper-nucleus total cross section, mb, for –									
	He	C	O	Al	A	Fe	Br	Ag	Ba	Pb
100	2251	3134	3243	4184	5123	5392	5981	6841	7545	8830
125	2200	3077	3190	4115	5036	5314	5903	6754	7453	8733
150	2171	3044	3160	4076	4987	5270	5860	6706	7401	8680
175	2118	2984	3104	4004	4900	5189	5779	6617	7307	8581
200	2046	2903	3029	3910	4786	5083	5673	6500	7183	8451
225	2002	2856	2985	3854	4718	5020	5610	6431	7110	8373
250	1967	2817	2948	3808	4663	4969	5558	6374	7050	8310
275	1935	2782	2916	3768	4615	4924	5513	6325	6997	8255
300	1915	2761	2896	3743	4586	4896	5485	6294	6965	8221
350	1898	2743	2880	3723	4561	4873	5462	6269	6938	8194
400	1894	2740	2877	3720	4558	4870	5459	6266	6935	8191
500	1942	2794	2927	3784	4636	4943	5532	6347	7020	8281
600	1991	2849	2979	3848	4714	5015	5606	6429	7105	8372
700	2018	2879	3008	3885	4758	5056	5648	6474	7154	8423
800	2040	2904	3031	3913	4792	5089	5681	6510	7192	8464
900	2057	2923	3050	3936	4820	5115	5707	6539	7222	8496
1000	2071	2939	3065	3954	4840	5135	5728	6562	7246	8521
1250	2094	2965	3090	3985	4875	5169	5763	6600	7286	8564
1500	2106	2980	3105	4001	4894	5189	5783	6621	7309	8589
1750	2116	2991	3117	4014	4908	5203	5798	6637	7326	8607
2000	2124	3000	3126	4025	4920	5215	5811	6651	7341	8623
2500	2129	3006	3134	4032	4927	5224	5821	6661	7351	8634
3000	2127	3005	3133	4030	4923	5222	5819	6659	7349	8632
3500	2124	3002	3130	4027	4918	5217	5815	6654	7344	8627
4000	2120	2997	3126	4021	4912	5211	5809	6648	7337	8620
5000	2114	2991	3120	4014	4903	5203	5801	6639	7328	8610
6000	2109	2985	3115	4007	4894	5195	5793	6630	7318	8600
7000	2102	2978	3108	3998	4884	5185	5783	6619	7307	8589
8000	2097	2972	3103	3991	4876	5178	5776	6611	7298	8580
9000	2094	2969	3100	3988	4871	5174	5773	6607	7294	8575
10000	2092	2968	3100	3986	4868	5173	5771	6605	7292	8574
12500	2090	2966	3100	3985	4865	5171	5771	6605	7291	8573
15000	2088	2965	3100	3984	4862	5170	5770	6604	7290	8573
17500	2085	2963	3098	3980	4857	5167	5768	6600	7286	8569
20000	2082	2960	3096	3977	4853	5163	5765	6597	7282	8565
22500	2080	2959	3095	3976	4850	5162	5763	6595	7281	8564

TABLE 32.- COPPER-NUCLEUS ABSORPTION CROSS SECTION

Energy, MeV/amu	Copper-nucleus absorption cross section, mb, for –									
	He	C	O	Al	A	Fe	Br	Ag	Ba	Pb
100	1198	1651	1697	2194	2691	2812	3105	3549	3908	4557
125	1161	1610	1659	2145	2629	2756	3049	3487	3843	4488
150	1144	1590	1641	2121	2600	2729	3023	3457	3811	4456
175	1127	1571	1624	2098	2572	2704	2998	3429	3782	4425
200	1113	1556	1610	2080	2549	2683	2977	3406	3757	4399
225	1103	1543	1599	2065	2531	2666	2960	3388	3738	4379
250	1094	1534	1590	2054	2517	2654	2948	3375	3724	4364
275	1089	1529	1585	2048	2509	2646	2941	3366	3715	4355
300	1087	1526	1583	2045	2505	2643	2938	3363	3711	4351
350	1088	1527	1584	2046	2506	2644	2939	3364	3712	4353
400	1093	1533	1590	2053	2515	2653	2948	3374	3722	4364
500	1122	1566	1621	2093	2564	2698	2993	3424	3775	4419
600	1148	1595	1648	2127	2606	2737	3032	3468	3821	4468
700	1162	1611	1663	2147	2630	2759	3054	3492	3847	4496
800	1172	1623	1674	2160	2647	2774	3070	3510	3865	4515
900	1180	1632	1682	2171	2659	2786	3082	3523	3879	4530
1000	1185	1638	1688	2178	2668	2794	3090	3532	3888	4540
1250	1192	1645	1696	2187	2678	2804	3100	3543	3900	4552
1500	1195	1650	1700	2191	2682	2809	3106	3549	3906	4559
1750	1198	1653	1704	2195	2686	2814	3111	3554	3911	4565
2000	1200	1656	1707	2198	2689	2817	3114	3557	3915	4569
2500	1201	1656	1708	2199	2689	2818	3116	3558	3916	4570
3000	1199	1655	1707	2197	2686	2815	3114	3556	3914	4568
3500	1197	1653	1705	2194	2682	2813	3111	3553	3910	4564
4000	1196	1651	1704	2192	2680	2810	3109	3550	3908	4562
5000	1194	1649	1702	2190	2677	2808	3106	3548	3905	4559
6000	1192	1647	1700	2187	2674	2805	3104	3544	3901	4555
7000	1190	1645	1698	2184	2670	2802	3100	3541	3898	4551
8000	1188	1643	1697	2183	2668	2800	3098	3539	3895	4549
9000	1188	1643	1697	2183	2667	2800	3099	3539	3895	4549
10000	1189	1644	1698	2183	2668	2800	3100	3540	3896	4550
12500	1191	1646	1701	2186	2670	2803	3103	3543	3900	4554
15000	1192	1648	1703	2187	2671	2805	3105	3545	3902	4557
17500	1192	1648	1704	2188	2671	2806	3106	3546	3903	4558
20000	1192	1648	1704	2188	2670	2806	3106	3546	3903	4558
22500	1193	1649	1705	2189	2671	2807	3108	3547	3904	4559

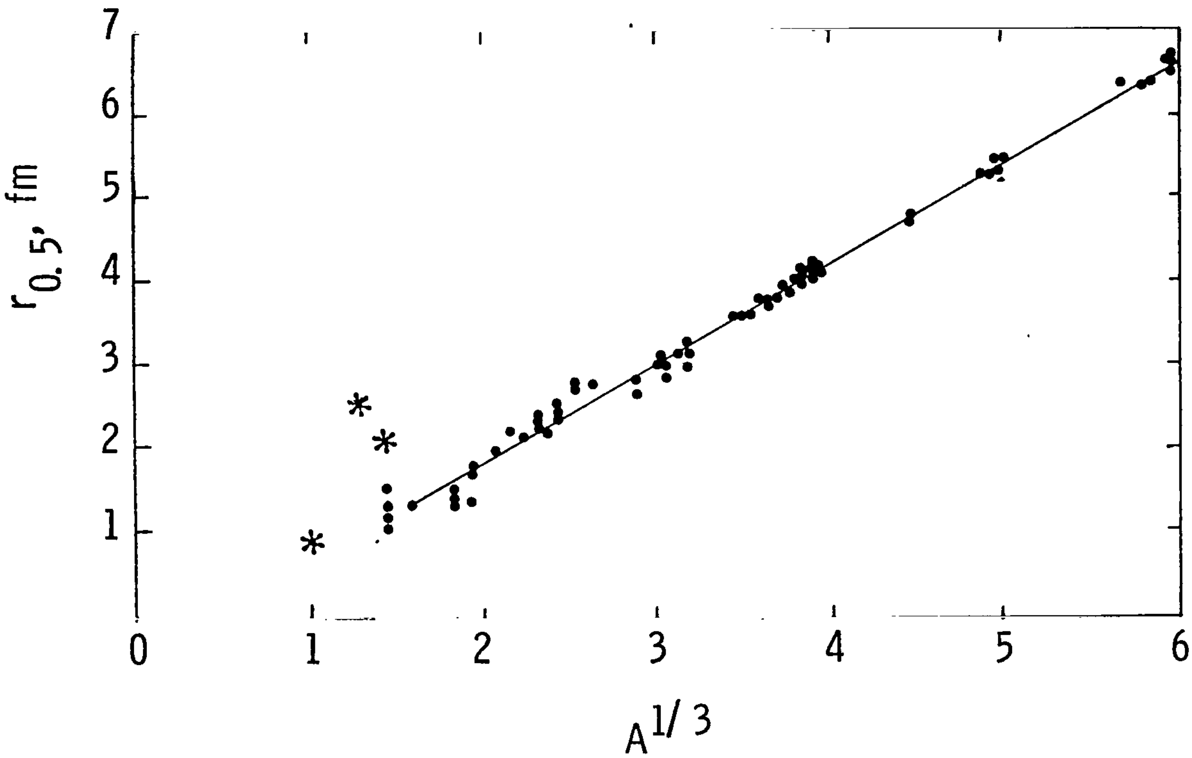

Figure 1.- Nuclear half-density radius as a function of mass number. Solid curve is used above He^4. Asterisks are values below He^4 obtained from assumed Gaussian density. Symbols are data tabulated by Hofstadter and Collard.

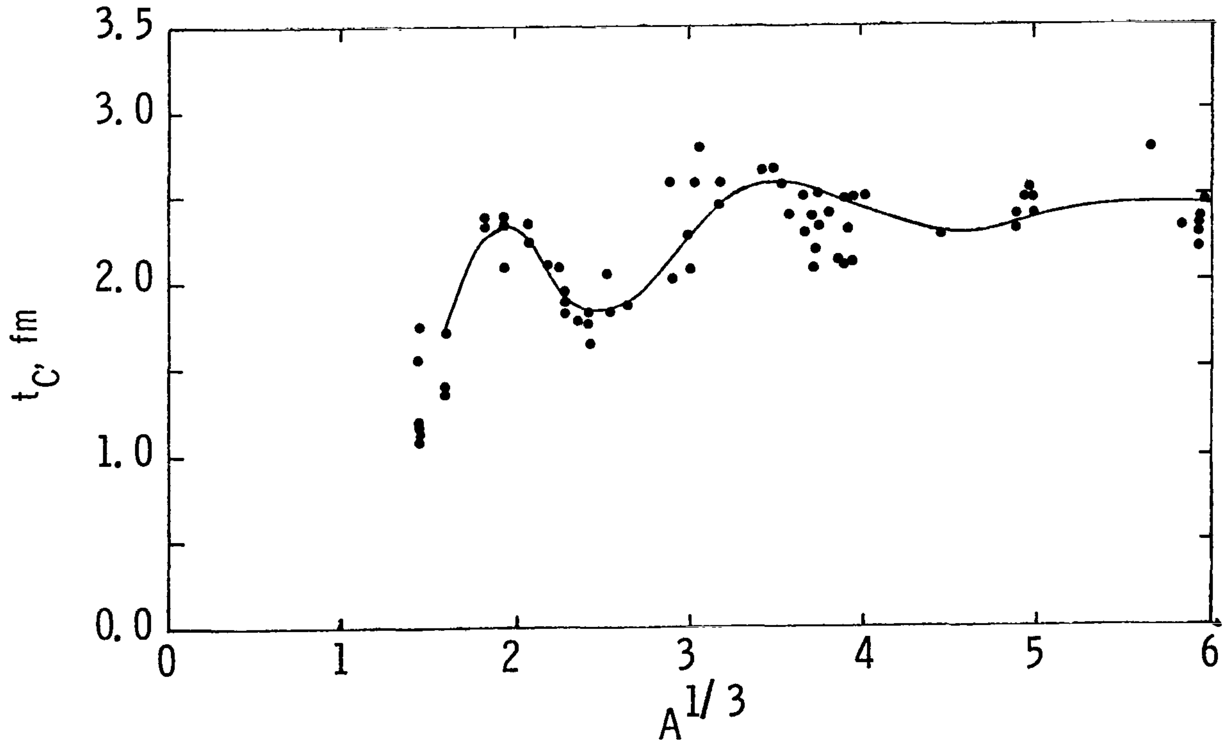

Figure 2.- Charge skin thickness as a function of mass number. Solid curve is used above He^4. Symbols are data tabulated by Hofstadter and Collard.

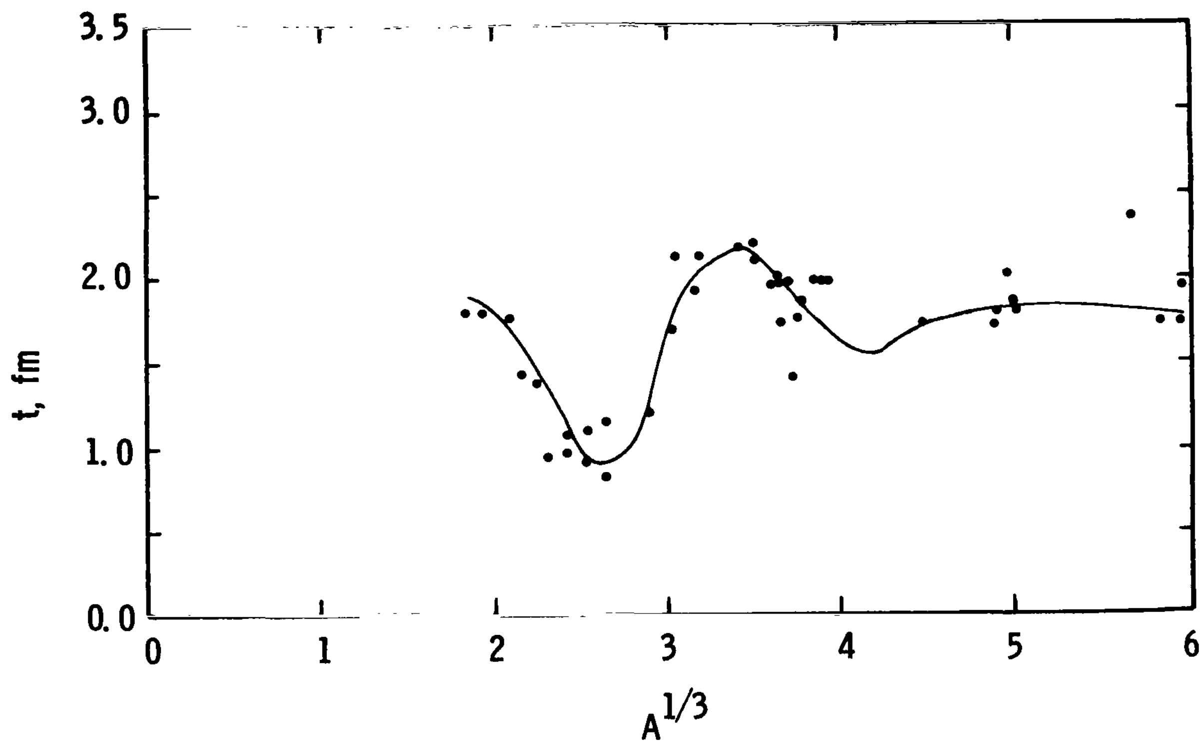

Figure 3.- Nuclear skin thickness as a function of mass number. Solid curve is used in calculations. Symbols are values determined from tabulated values of Hofstadter and Collard.

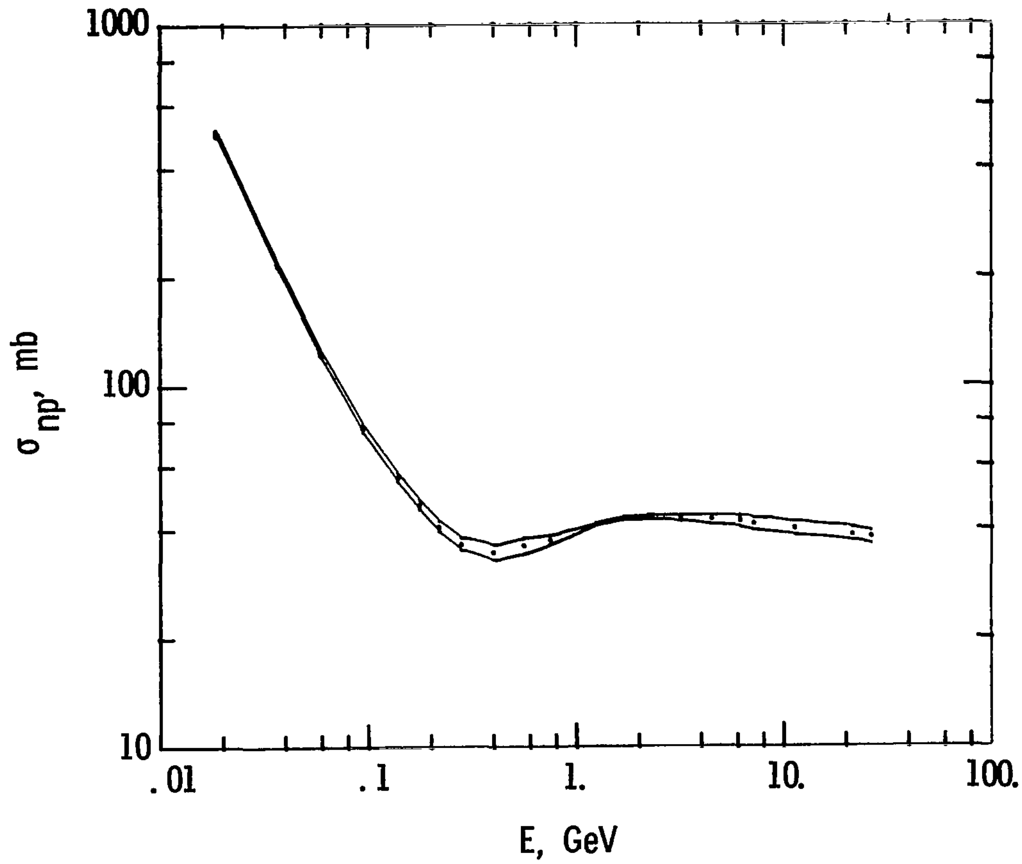

Figure 4.- Neutron-proton total cross section as a function of laboratory energy. The two curves give range of uncertainty.

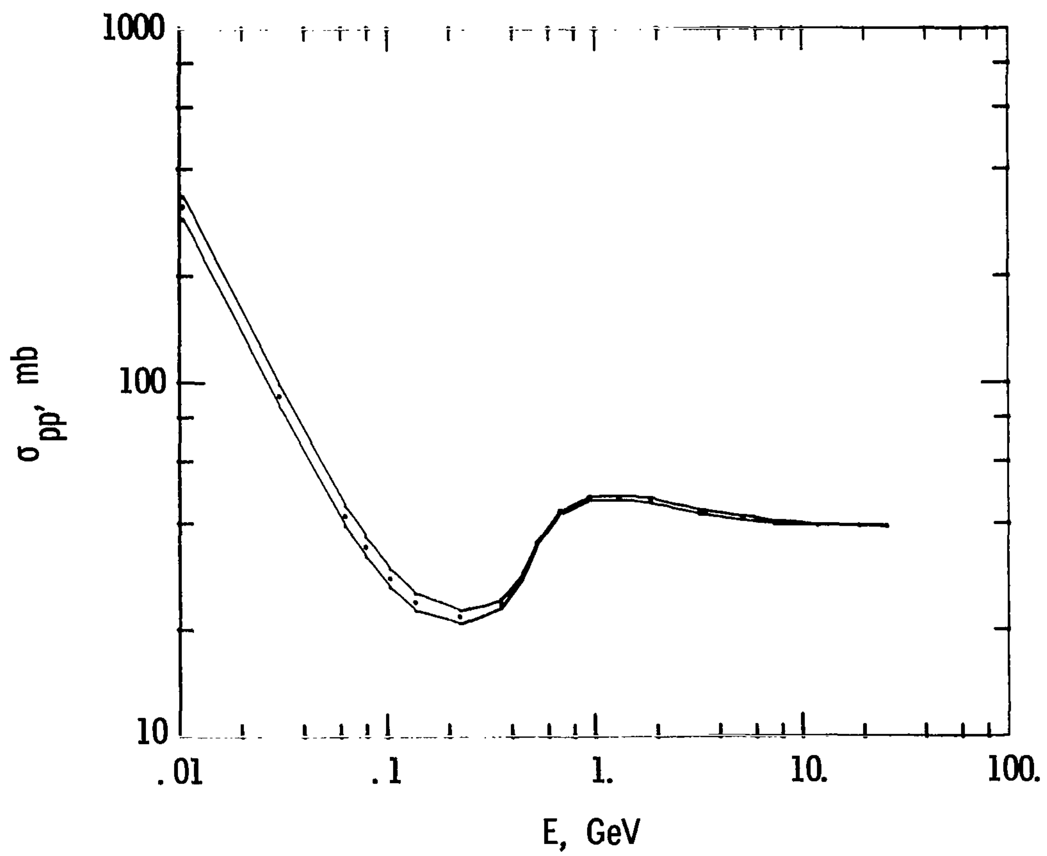

Figure 5.- Proton-proton total cross section as a function of laboratory energy. The two curves give range of uncertainty.

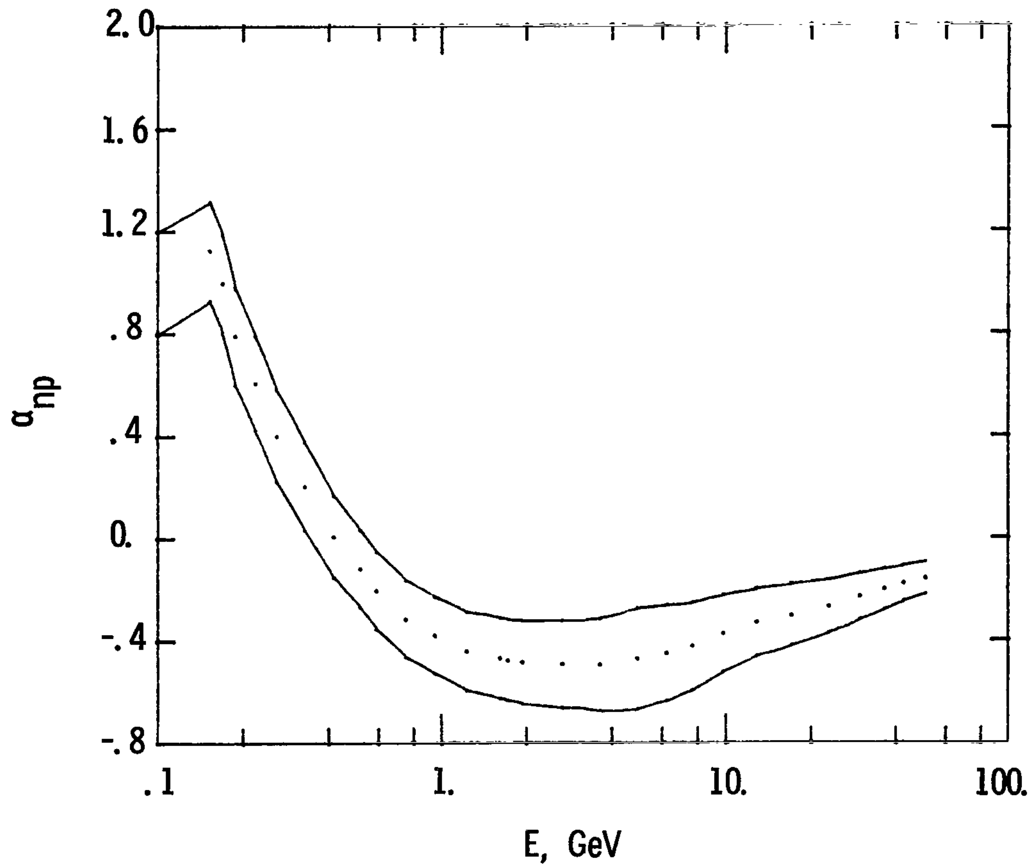

Figure 6.- Ratio of real to imaginary part of forward neutron-proton scattering amplitude as a function of laboratory energy. The two curves give range of uncertainty.

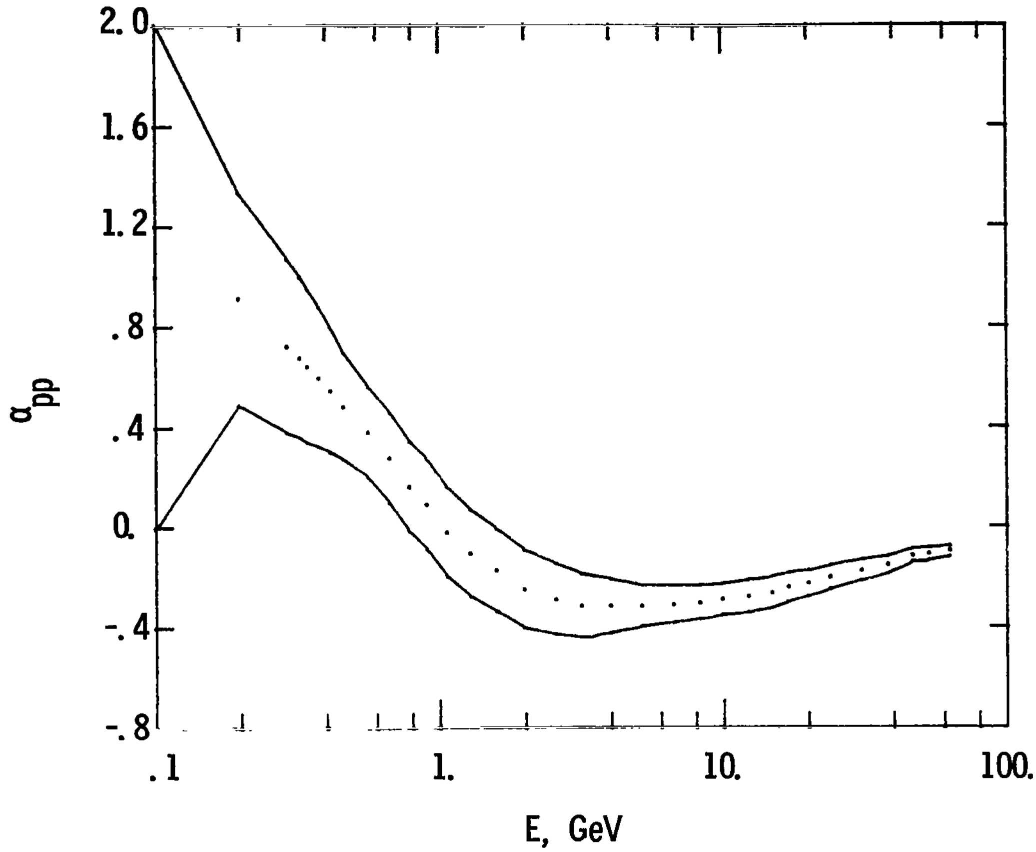

Figure 7.- Ratio of real to imaginary part of forward proton-proton scattering amplitude as a function of laboratory energy. The two curves give range of uncertainty.

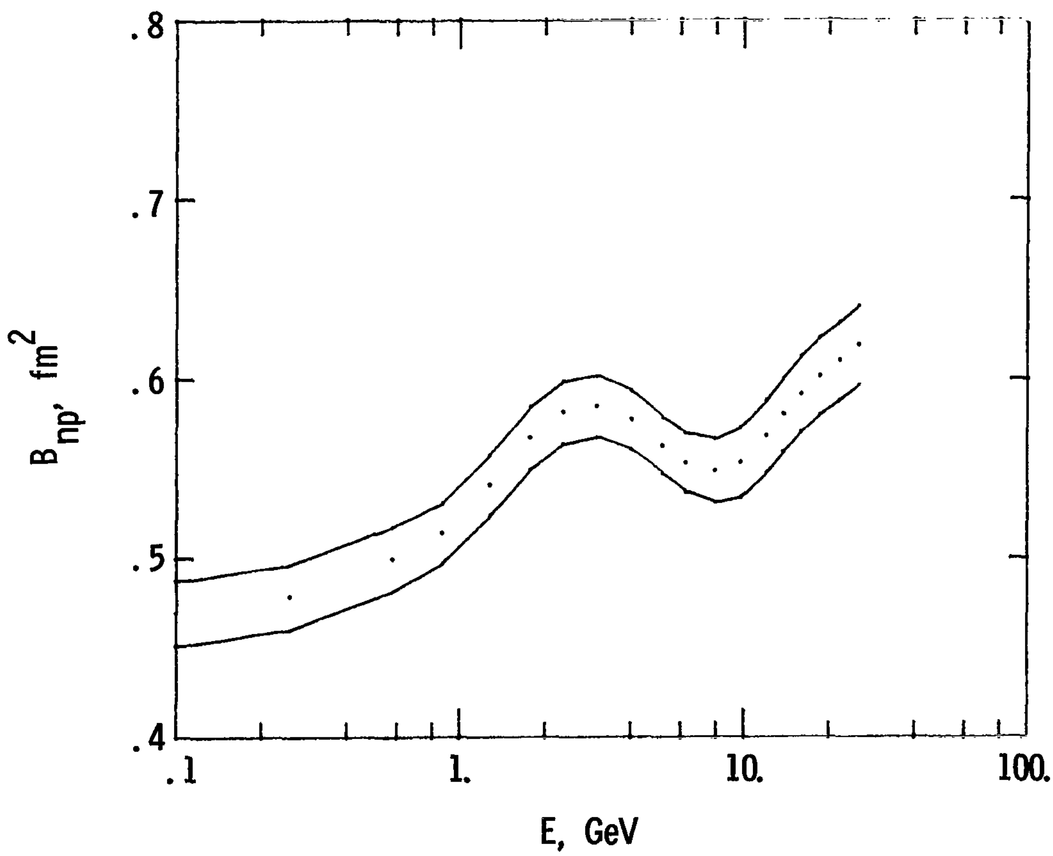

Figure 8.- Neutron-proton scattering slope parameter as a function of laboratory energy. The two curves give range of uncertainty.

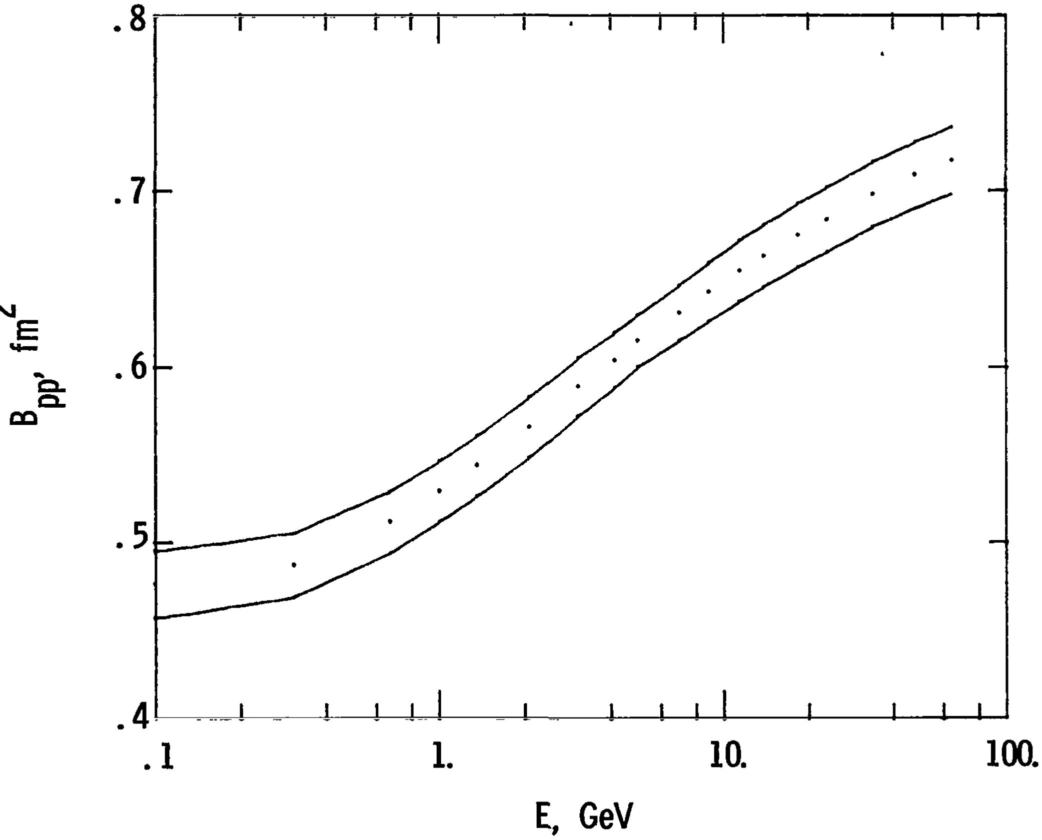

Figure 9.- Proton-proton scattering slope parameter as a function of laboratory energy. The two curves give range of uncertainty.

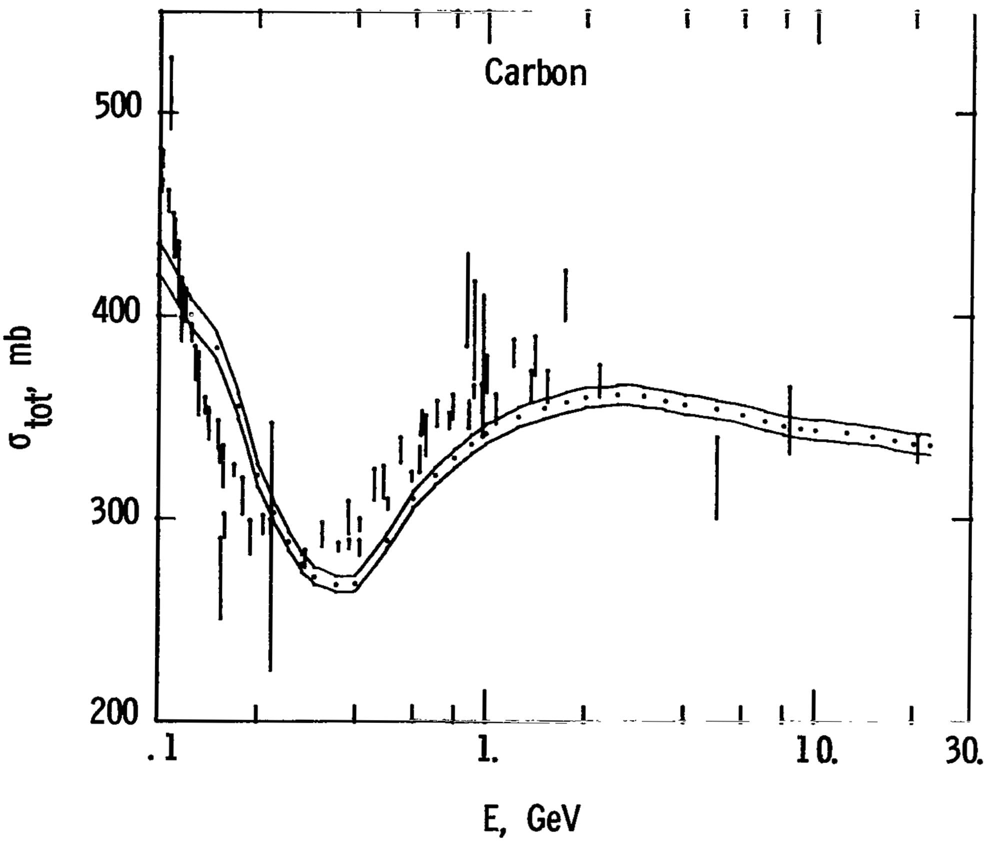

Figure 10.- Nucleon-carbon total cross section as a function of laboratory energy. The two curves give range of uncertainty.

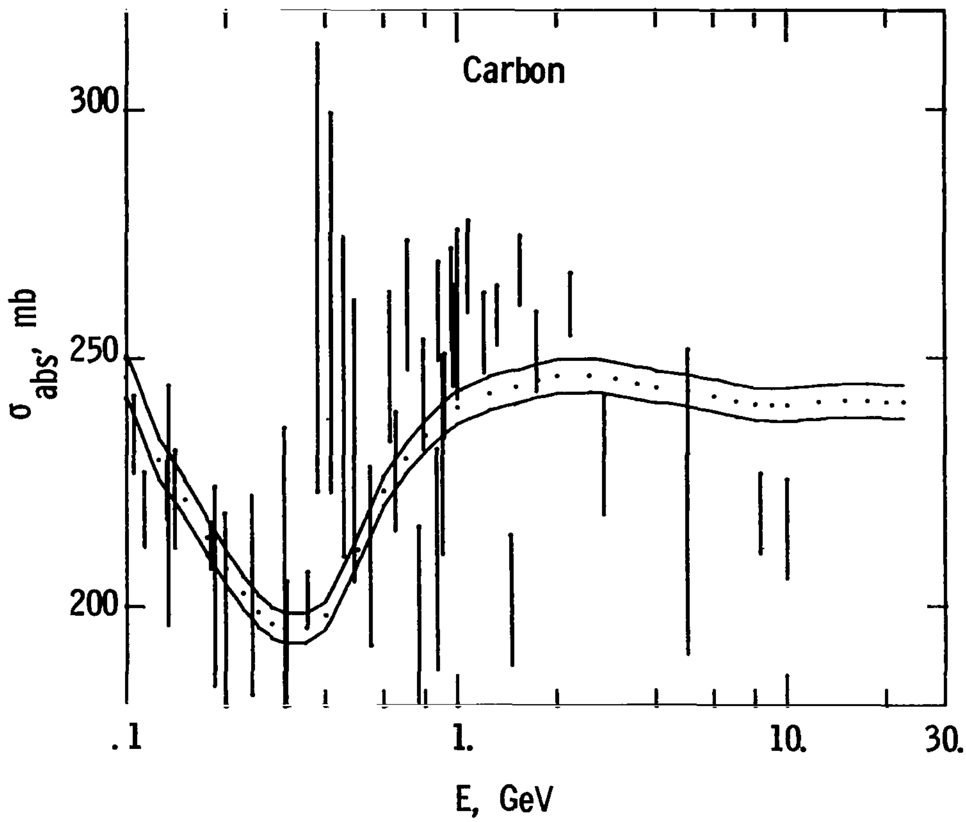

Figure 11.- Nucleon-carbon absorption cross section as a function of laboratory energy. The two curves give range of uncertainty.

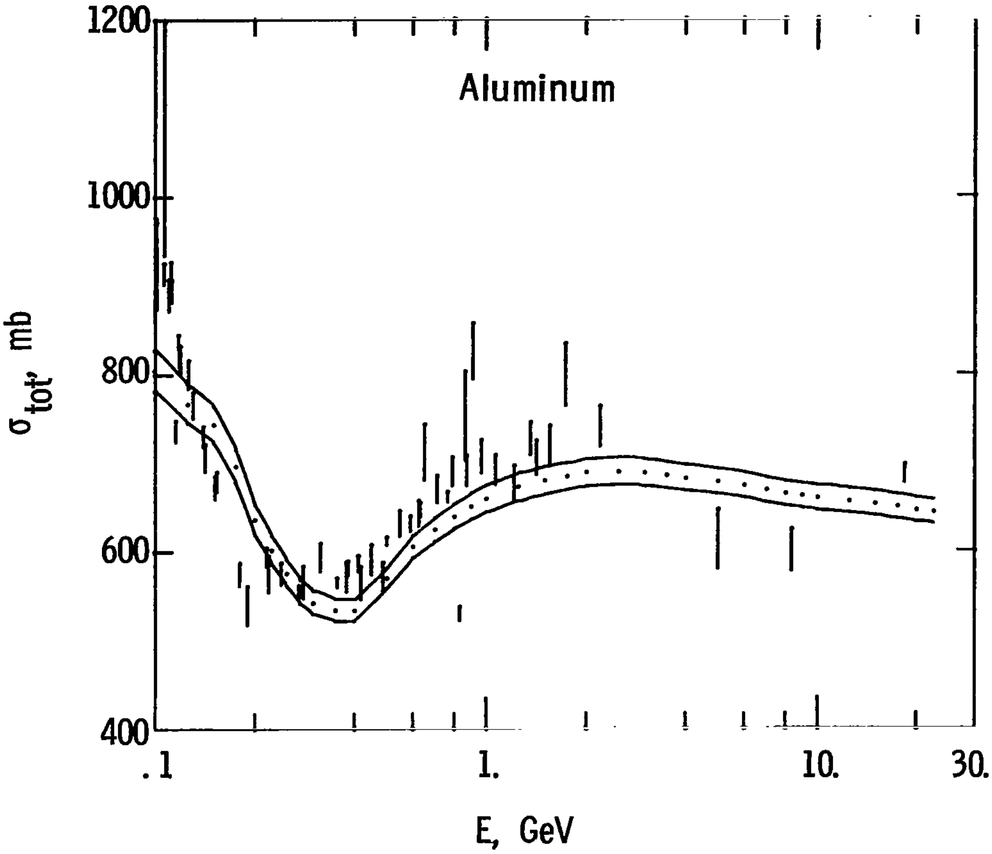

Figure 12.- Nucleon-aluminum total cross section as a function of laboratory energy. The two curves give range of uncertainty.

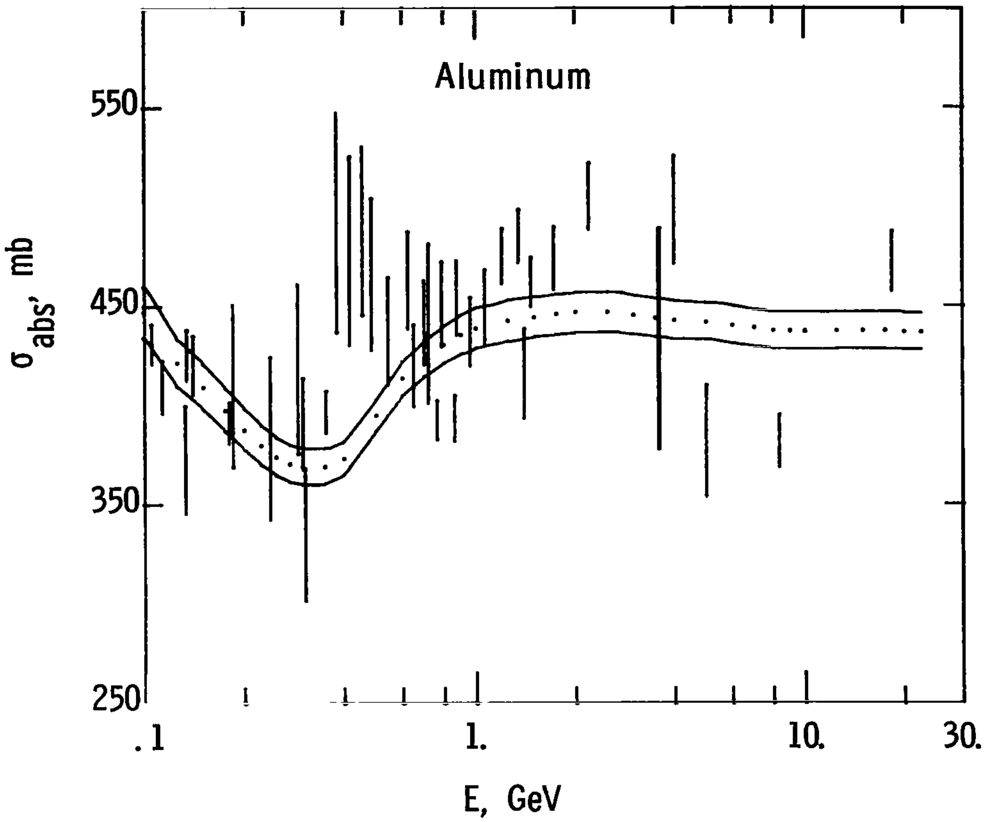

Figure 13.- Nucleon-aluminum absorption cross section as a function of laboratory energy. The two curves give range of uncertainty.

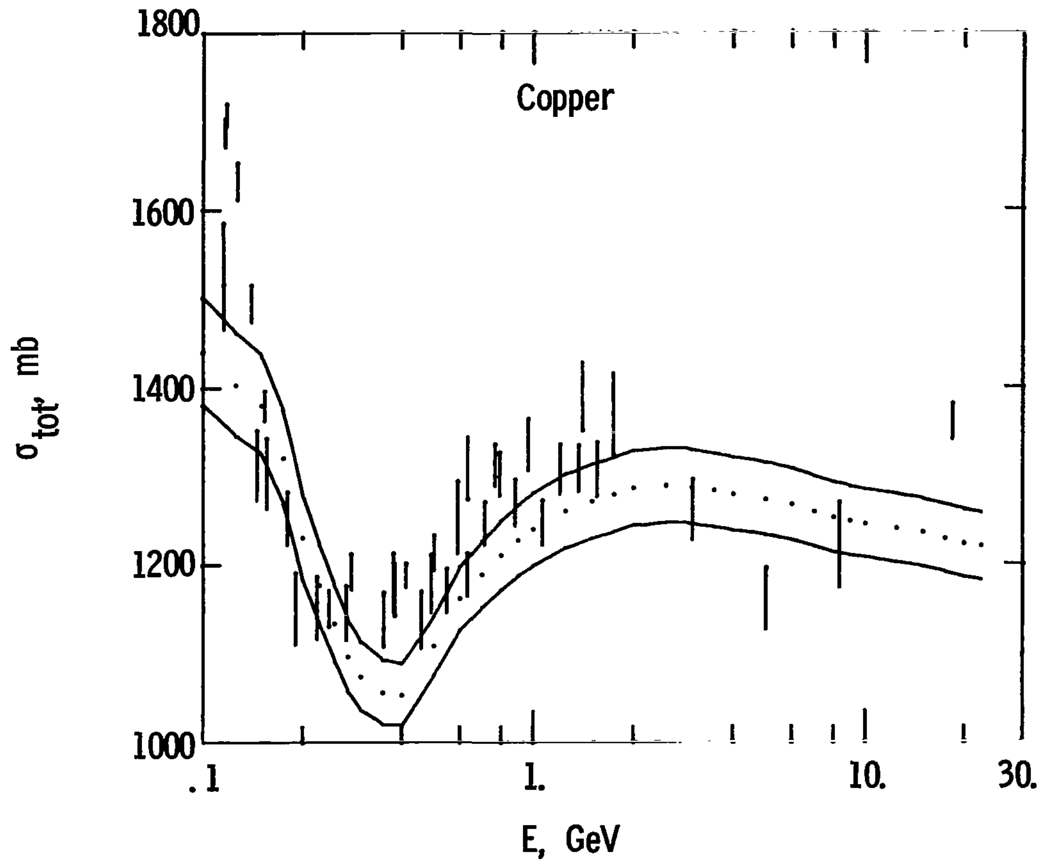

Figure 14.- Nucleon-copper total cross section as a function of laboratory energy. The two curves give range of uncertainty.

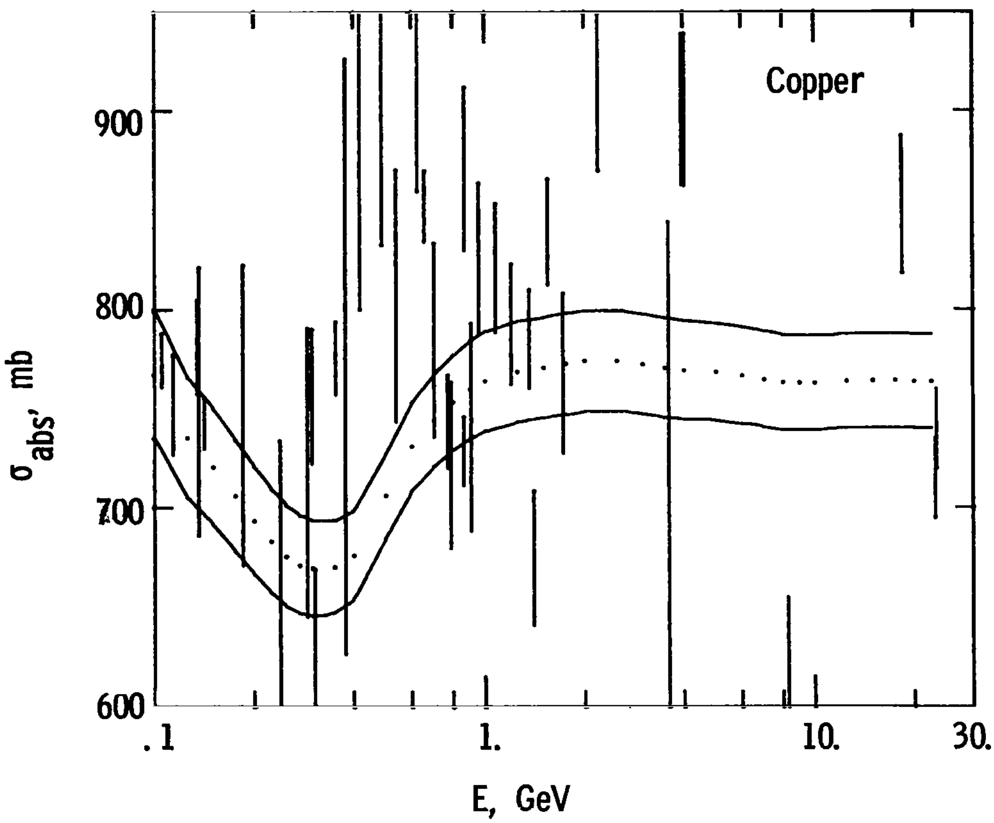

Figure 15.- Nucleon-copper absorption cross section as a function of laboratory energy. The two curves give range of uncertainty.

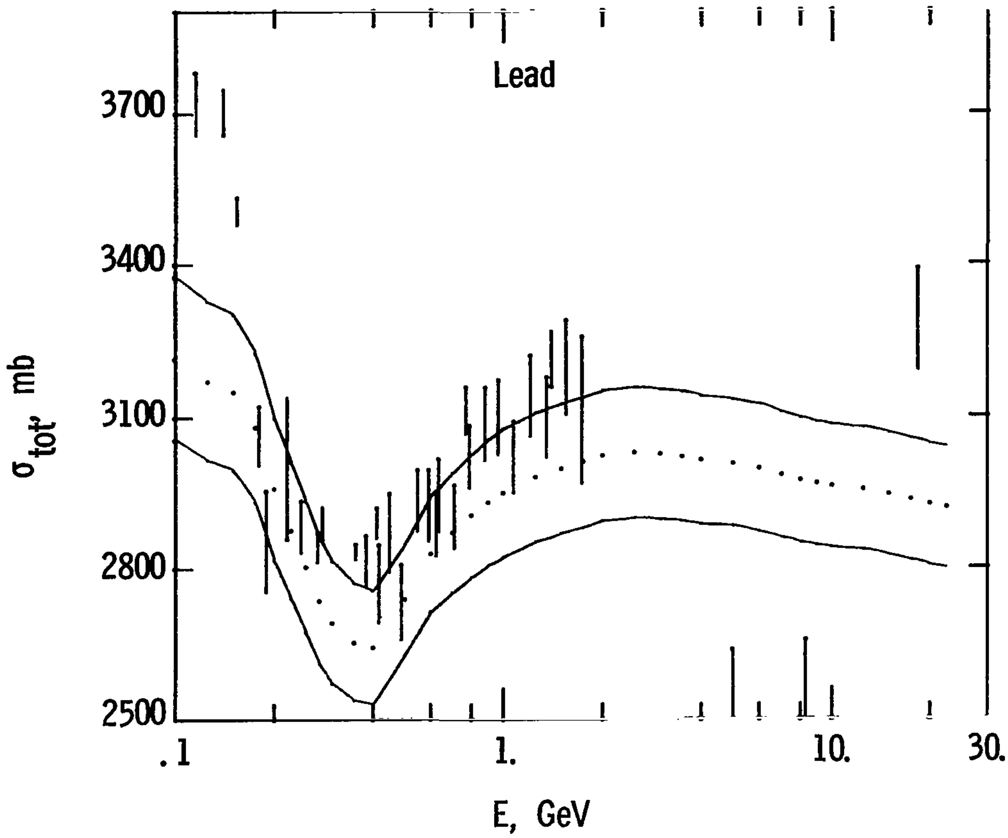

Figure 16.- Neutron-lead total cross section as a function of laboratory energy. The two curves give range of uncertainty.

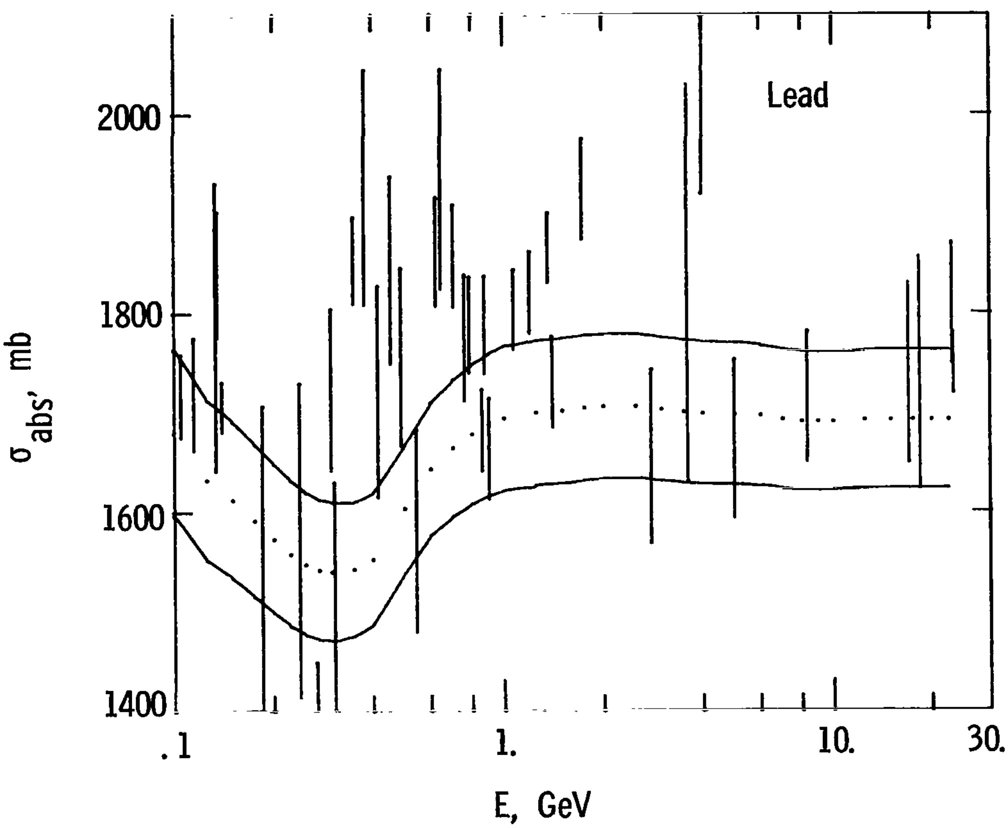

Figure 17.- Neutron-lead absorption cross section as a function of laboratory energy. The two curves give range of uncertainty.

NATIONAL AERONAUTICS AND SPACE ADMINISTRATION
WASHINGTON, D.C. 20546

OFFICIAL BUSINESS
PENALTY FOR PRIVATE USE $300

SPECIAL FOURTH-CLASS RATE
BOOK

POSTAGE AND FEES PAID
NATIONAL AERONAUTICS AND
SPACE ADMINISTRATION
451

U.S.MAIL

154 001 C1 U H 751219 S00903DS
DEPT OF THE AIR FORCE
AF WEAPONS LABORATORY
ATTN: TECHNICAL LIBRARY (SUL)
KIRTLAND AFB NM 87117

POSTMASTER: If Undeliverable (Section 158 Postal Manual) Do Not Return

"The aeronautical and space activities of the United States shall be conducted so as to contribute . . . to the expansion of human knowledge of phenomena in the atmosphere and space. The Administration shall provide for the widest practicable and appropriate dissemination of information concerning its activities and the results thereof."

—NATIONAL AERONAUTICS AND SPACE ACT OF 1958

NASA SCIENTIFIC AND TECHNICAL PUBLICATIONS

TECHNICAL REPORTS: Scientific and technical information considered important, complete, and a lasting contribution to existing knowledge.

TECHNICAL NOTES: Information less broad in scope but nevertheless of importance as a contribution to existing knowledge.

TECHNICAL MEMORANDUMS: Information receiving limited distribution because of preliminary data, security classification, or other reasons. Also includes conference proceedings with either limited or unlimited distribution.

CONTRACTOR REPORTS: Scientific and technical information generated under a NASA contract or grant and considered an important contribution to existing knowledge.

TECHNICAL TRANSLATIONS: Information published in a foreign language considered to merit NASA distribution in English.

SPECIAL PUBLICATIONS: Information derived from or of value to NASA activities. Publications include final reports of major projects, monographs, data compilations, handbooks, sourcebooks, and special bibliographies.

TECHNOLOGY UTILIZATION PUBLICATIONS: Information on technology used by NASA that may be of particular interest in commercial and other non-aerospace applications. Publications include Tech Briefs, Technology Utilization Reports and Technology Surveys.

Details on the availability of these publications may be obtained from:

SCIENTIFIC AND TECHNICAL INFORMATION OFFICE

NATIONAL AERONAUTICS AND SPACE ADMINISTRATION

Washington, D.C. 20546